The Vulnerability of Nigral Dopamine Neurons to Mitochondrial Complex I Deletion in the Adult Mouse: Implications for Parkinson's Disease Pathogenesis

Noah Sorscher

A dissertation,

submitted in partial fulfillment of the

requirements for the degree of

Doctor of Philosophy

University of Washington

2012

Reading Committee:

Zhengui Xia, Chair

Rick Morrison

Jing Zhang

Program Authorized to Offer Degree:

Neurobiology & Behavior

University of Washington

Abstract

The Vulnerability of Nigral Dopamine Neurons to Mitochondrial Complex I Deletion in the Adult Mouse: Implications for Parkinson's Disease Pathogenesis

Noah Sorscher

Chair of the Supervisory Committee:
Professor Zhengui Xia
Department of Environmental and Occupational Health Sciences

Parkinson's disease (PD) is a neurodegenerative movement disorder, characterized by the motor symptoms of tremor, rigidity, postural instability and slowness of movement. These motor symptoms are caused by the death of the dopamine-producing neurons in the substantia nigra (SN) of the midbrain, however the underlying cause of this selective neurodegeneration is unknown. Many lines of evidence support a causative role for mitochondria in this dopaminergic cell death, and specifically the inhibition of complex I of the electron transport chain. Here we show that the specific removal of complex I function from the mouse does not produce a loss of dopaminergic cell bodies like that seen in PD, nor does it produce a loss of the dopamine-producing protein tyrosine hydroxylase (TH) in the striatum. These data suggest that inhibition of complex I is not sufficient to account for the selective dopaminergic cell death of PD. However, we did observe significant axonal dystrophy in dopaminergic axons, and a reduction of mitochondrial size consistent with decreased mitochondrial fusion, both of which are implicated in PD pathogenesis. Although it remains to be determined whether these effects are specific to dopamine neurons, these data are consistent with a cooperative role for complex I inhibition in the degeneration of the nigrostriatal pathway and the loss of dopaminergic axons.

Table of Contents

List of Figures

Chapter 1

INTRODUCTION

Parkinson's disease

Patients with Parkinson's disease (PD) experience characteristic motor symptoms of tremor, rigidity, slowness of movement, and postural instability, as well as many other symptoms of varying severity, both physical and psychological (Jain and Goldstein, 2012). PD is characterized by the formation of proteinaceous inclusion bodies called Lewy bodies, and by a progressive degeneration of the dopaminergic neurons of the substantia nigra (SN) innervating the striatum, which contributes to planning movements and modulating executive function. The loss of dopamine neurons in the SN is sufficient to produce the hallmark motor symptoms of PD, although degeneration also occurs in other brain regions (Braak et al., 2003). No cure exists, and the current standard of care is dopamine replacement therapy, which does not slow the progressive degeneration. Intractable PD cases are often treated with deep brain stimulation, in which a stimulating electrode is surgically implanted primarily in the sub-thalamic nucleus (STN). The electrode is believed to activate the inhibitory afferents decreasing the output activity of the STN (Gradinaru et al., 2009). However even this extreme intervention has not been shown to slow disease progression (Sidiropoulos et al., 2012) despite promising early trends to the contrary (Tagliati et al., 2010). Because there is no therapy to slow or reverse disease progression, elucidating the causal factors is paramount in PD research. Although the cause of the progressive selective dopaminergic

neurodegeneration in non-heritable (sporadic) PD is unknown, many theories have been proposed including mitochondrial dysfunction (Schapira, 2011), pesticide exposure (Moretto and Colosio, 2011; Wirdefeldt et al., 2011), oxidative stress (Henchcliffe and Beal, 2008; Jenner, 2003), protein misfolding (Olanow and McNaught, 2011), excitotoxicity (Caudle and Zhang, 2009), metal exposure (Wirdefeldt et al., 2011), inflammation (Barnum and Tansey, 2010), differential expression of calcium channels (Hurley and Dexter, 2012), and the theory of synergy between several of these causes (Carvey et al., 2006). There is also a possibility that PD represents a multitude of independent conditions with different causes, convergent on the selective or even arbitrary destruction of the SN.

Roughly 10% of all cases of PD are attributable to genetic mutations, and the rest of cases are sporadic. Many of the genetic forms fall into the category of autosomal recessive juvenile-onset Parkinsonism (AR-JP), rather than the late adult onset of the sporadic form of PD. The divergence of these AR-JP symptoms from the more common sporadic form predicts that their mechanism of onset could be different as well. However, they are extremely useful for providing a window into possible explanations of the selective vulnerability of dopamine neurons. The most common genetic forms of PD are caused by mutations in the genes α-synuclein, parkin, leucine-rich repeat kinase 2 (LRRK2), PTEN-induced putative kinase 1 (PINK1), DJ-1, and ATP13A2 (Lesage and Brice, 2009). Of these, PINK1 and DJ-1 encode proteins targeted to mitochondria, and parkin has been found to be recruited to the mitochondria by PINK1, and to regulate mitochondrial synthesis and degradation, the latter by a process known as mitophagy (Castillo-Quan, 2011). Furthermore, the PD-linked mutations of α-

synuclein were found to result in mitochondrial degeneration (Martin et al., 2006) and interference with mitochondrial functions (Devi et al., 2008), and the α-synuclein protein was found to contain a non-canonical mitochondrial targeting signal (Devi et al., 2008). The functioning of mitochondria has also been found to be impaired as a result of the pathogenic forms of LRRK2 (Mortiboys et al., 2010) and ATP13A2 (Grunewald et al., 2012).

Mitochondria

Many independent lines of research suggest an integral role for mitochondria in the pathogenesis of PD. The first chemical agent discovered to cause selective and permanent dopaminergic degeneration of the central nervous system when applied systemically in animals, and indeed the only agent demonstrated to reliably cause this condition in humans, MPTP (Langston et al., 1983; Langston and Ballard, 1983), was discovered to act as an inhibitor of mitochondrial complex I (Nicklas et al., 1987). Mitochondrial complex I, or NADH dehydrogenase, is the first and largest protein complex of the electron transport chain (ETC), which along with ATP synthase carries out the process of oxidative phosphorylation. It was later discovered that another complex I inhibitor, rotenone, could also mimic the Parkinsonian phenotype in laboratory animal models (Alam and Schmidt, 2002; Betarbet et al., 2000; Marella et al., 2008), although the selectivity of rotenone for dopamine neurons has been contentious (Cicchetti et al., 2009; Greenamyre et al., 2010; Hoglinger et al., 2006; Schmidt and Alam, 2006). While MPTP's selectivity for dopamine neurons comes from being a substrate of the dopamine transporter (Javitch et al., 1985; Pifl et al.,

1993), rotenone freely crosses the plasma membrane of all cells, and inhibits complex I systemically. The observation that dopamine neurons appear to harbor a selective vulnerability to both of these inhibitors, but by dissimilar mechanisms of selectivity, supports the hypothesis that complex I inhibition is sufficient to produce the characteristic selective neurodegeneration of PD (Betarbet et al., 2000).

The hypothesis was further strengthened when it was shown that the dopaminergic degeneration from MPTP and rotenone could be prevented by transgenic over-expression of the analogous NADH dehydrogenase from yeast, NDI1 (Marella et al., 2008; Seo et al., 2006). NDI1 is a single-polypeptide NADH dehydrogenase, which differs from mammalian complex I in that it is not inhibited by MPTP or rotenone. It also differs in that it does not translocate protons across the mitochondrial inner membrane (Perales-Clemente et al., 2008), but like complex I it does transfer electrons from NADH to ubiquinone, the next electron carrier in the ETC. The concurrent restoration of dopamine cell survival and the ETC, in spite of MPTP or rotenone, seemed to corroborate of the idea that the inhibition of the role of complex I in the ETC was obligatory for the selective death of dopamine neurons in the MPTP and rotenone models of PD.

Mitochondrial involvement in PD is also implicated by several of the genes responsible for genetic forms of PD. Though not confirmed *in vivo*, it was reported *in vitro* that DJ-1 binds to complex I and is necessary for complex I function (Hayashi et al., 2009; Heo et al., 2012). Prior to this, DJ-1 has been believed to function as a sensor of oxidative stress (Cookson, 2010).

Much of the research linking familial PD and mitochondria however is not specific to complex I. In *drosophila*, PINK1 and parkin proteins were reported to act in a shared molecular signaling pathway (Pallanck, 2010), which participates in maintaining the balance of mitochondrial dynamics, the twin processes of fission and fusion that allow mitochondria to mediate a continual interchange of components and material while maintaining their size and structure. Recently the field of mitochondrial dynamics has surged with respect to neurodegenerative disease. Mitochondria experience a complex dynamic equilibrium between fission and fusion, wherein the individual mitochondrial particles of the cell are not isolated or stationary, but rather undergo a continual ballet of combining and dividing. The reason for this extensive dynamism is still being explored, but a number of functions have been uncovered through which mitochondrial dynamics can enhance a cell's fitness. Sharing DNA between mitochondria to compensate for mutation (Nakada et al., 2001), dimerization of ATP synthase on the inner mitochondrial membrane (Gomes et al., 2011), and increasing the efficiency of energy production (Blackstone and Chang, 2011) have been proposed benefits. Mitochondrial dynamics have also been shown to adjust mitochondrial size and segregate damaged proteins to better facilitate autophagy (Twig et al., 2008) and for transport along axons (Ishihara et al., 2009), both of which may have implications for neurodegeneration. The PINK1/parkin pathway has been proposed to preferentially segregate damaged mitochondria and isolate them from further fusion, so they can be degraded (Pallanck, 2010). In an independent pathway, parkin was shown to indirectly regulate the transcription of

PGC-1α, a transcriptional coactivator with an important role in mitochondrial biogenesis (Shin et al., 2011).

The PINK1/parkin pathway of mitochondrial clearance is reported to be initiated by reduced mitochondrial membrane potential (Pallanck, 2010). It was also reported that DJ-1 acts in parallel to perform similar functions (Thomas et al., 2011). While a reduction of mitochondrial membrane potential can result from complex I inhibition, it also can be the result of inhibition of complex III or IV. And furthermore, the rescue of MPTP and rotenone intoxication by NDI1, an NADH dehydrogenase that does not translocate protons across the mitochondrial membrane, suggests that the membrane polarization capacity of complex I is dispensable. Conversely, direct disruption of the fission-fusion balance can itself produce a deficit of oxidative phosphorylation (Van Bergen et al., 2011). Therefore, while the roles of PD genes are consistent with the complex I hypothesis of PD pathogenesis, they don't specifically support it.

Mitochondrial function may also be regulated by α-synuclein, a gene linked with familial PD as well as a major protein component of Lewy bodies (Spillantini et al., 1997). It has been reported that α-synuclein drives mitochondrial fission (Nakamura et al., 2011), although it does so by directly altering the mitochondrial membrane, not by regulating the proteins that ordinarily mediate mitochondrial dynamics (Nakamura et al., 2011). α-Synuclein was also shown to enter mitochondria using a non-canonical targeting signal (Devi et al., 2008), and from there to inhibit complex I activity and increase reactive oxygen species (Devi et al., 2008). However it was later reported that this inhibition is not related to α-synuclein's pathological potential (Loeb et al., 2010). Finally, it

was found that α-synuclein's mitochondrial function may be triggered in response to acidification of the cytoplasm (Cole et al., 2008). This may suggest a position for α-synuclein as part of a reaction to other pathological conditions within the cell, reminiscent of the models in which DJ-1 responds to oxidation state and in which PINK1 and parkin respond to loss of mitochondrial membrane polarization. While the evidence grows that α-synuclein plays an important role in mitochondrial processes, including but not exclusive to complex I, the implications of this relationship remain unclear.

Mouse model

The goal of this study was to determine whether the genetic removal of complex I function is sufficient to produce dopaminergic neurodegeneration consistent with a model of PD *in vivo*. Despite previous evidence suggesting the necessity of complex I function in the survival of dopamine neurons, it was demonstrated by our lab that the direct genetic ablation of complex I function in cultured dopaminergic primary neurons did not affect the level of survival or apoptosis (Choi et al., 2008). Although this seems to contradict the hypothesis that complex I inhibition can result in the degeneration of dopamine neurons, it could still be argued that the time course of dopamine neuron degeneration needs simply to be longer than it is possible to maintain primary dopamine neurons in culture. The rotenone model of dopamine degeneration in rats and mice does not take effect until 4 weeks after the beginning of treatment (Betarbet et al., 2000; Inden et al., 2007), and reports suggest that it is even more disease relevant after 8 weeks (Inden et al., 2011). In this study, we use an *in vivo* model

of complex I deletion, which allows us to extend the experimental time course for up to 5 months.

Our *in vivo* strategy of genetic complex I deletion also permits us to access other parameters of dopamine neuron vulnerability. It could be argued that interaction with glia or other neurons mediates an elevated dependency on complex I function, and *in vivo* neurons can be expected to form synapses and interact with glia in ways that are out of reach in culture. The physiological role of glia is necessary to the dopamine degeneration from MPTP, and has been proposed to contribute to idiopathic PD (Barnum and Tansey, 2010). And the pattern of neuronal activity has been proposed to contribute to the degeneration in PD (Caudle and Zhang, 2009; Hurley and Dexter, 2012). Furthermore it has been argued that the degeneration of dopamine axons, rather than cell bodies, is the primary determinant of clinically apparent progression of PD (Cheng et al., 2010). By studying the dependence of dopamine neurons on complex I *in vivo*, we are able to address these concerns.

Genetic deletion of complex I function is accomplished by knocking out the gene *ndufs4* (Choi et al., 2008; Kruse et al., 2008; Quintana et al., 2010). NDUFS4 is one of over 40 protein subunits that comprise complex I, and without NDUFS4 complex I fails to assemble or function (Budde et al., 2000; Scacco et al., 2003; van den Heuvel et al., 1998). Mutations in *ndufs4* in humans result in Leigh syndrome (Assouline et al., 2012), which progresses rapidly with a life expectancy of about 1 year. Symptoms of tremor and rigidity have been reported in Leigh syndrome (Macaya et al., 1993). Mutations in another complex I subunit gene, *ndufv2*, was suggested to correlate with a mild form of PD, but the result

was inconclusive due to small sample size (Nishioka et al., 2010). In mice with *ndufs4* deletion, developing juveniles experience severe dystonia, hypoactivity, failure to thrive, motor deficits, and ultimately die at around 50 days after birth (Kruse et al., 2008). The cause of death is suspected to be respiratory failure, associated with inflammation in the vestibular nuclei of the brainstem (Quintana et al., 2012), and restoration of *ndufs4* in this nucleus can prolong their lifespan (Quintana et al., 2012). This severe developmental phenotype interferes with the ability to conduct experiments on adult, developed animals that might be vulnerable to progressive neurodegeneration. It is for this reason that the inducible knockout (Quintana et al., 2010) was chosen for this study. In the inducible *ndufs4* knockout, mice express the Cre recombinase protein but it remains inactive until stimulated by the drug tamoxifen. Upon exposure to tamoxifen, the Cre protein enters the nucleus and excises the second exon of the *ndufs4* gene, which results in a premature stop codon. The mice also carry a reporter gene, *LacZ* preceded by a floxed-stop codon, so that upon Cre activation the *LacZ* will become subject to gene transcription. In this study, the mice are phenotypically normal until they are adults at 12 weeks after birth, at which point tamoxifen is administered, inducing Cre activation and *ndufs4* deletion. Mice lacking the Cre gene are also treated with tamoxifen, and used as wild type controls. This allows us to avoid the severe developmental disorders resulting from the conventional *ndufs4* knockout, and it also allows us to exclude the possibility that differences we observe were due to developmental compensation.

Using this mouse, we examined whether the genetic deletion of complex I in adults produces any degeneration of dopamine neurons of the SN. Specifically we examined the induced *ndufs4* knockout mice for behavioral phenotypes and the loss of dopaminergic cell bodies in the SN characteristic of PD. In addition, to determine whether loss of complex I activity affects the axon integrity in the striatum or mitochondrial dynamics of dopamine neurons, we analyzed the staining intensity and structure of dopamine axons, and the size and shape of mitochondria of the TH+ neurons in the SN, from wild type and induced *ndufs4* knockout mice.

Chapter 2

RESULTS

These results fall into 5 categories: (1) verification of the induced *ndufs4* knockout, (2) testing of dopamine-dependent motor deficits, (3) measuring the survival of dopamine cell bodies in the substantia nigra (SN), (4) assessing the preservation and structure of dopamine axons in the striatum, and (5) examining mitochondrial morphology for evidence that there had been a shift in mitochondrial dynamics after the induced knockout of *ndufs4*.

Knockout induction was verified in adult animals. Animals age 12-13 weeks were administered tamoxifen (250 mg/kg body weight) for 10 days, to activate the ER^{t2} receptor and thereby induce the knockout of the *ndufs4* gene. To determine whether tamoxifen stimulation had resulted in reduced levels of NDUFS4 protein expression we performed western blot analysis on whole brain lysates from induced *ndufs4* knockout animals and wild type littermate controls. We found that the levels of NDUFS4 protein in tissues of induced knockout animals were significantly decrease compared with wild type littermates (Fig. 1A).

To assess whether the activity of complex I was similarly reduced, isolated mitochondria from whole brains were analyzed for the rate of oxygen consumption using the polarography method (Tieu et al., 2003). The rate of decline in oxygen was recorded after adding the substrates necessary for complex I function, and compared to the rate of oxygen decrease after inactivating complex I by the addition of rotenone. We found that the complex I-

dependent rate of oxygen consumed was significantly slower from induced knockout tissues than from wild type littermate controls (Fig. 1B).

To examine the pattern of Cre recombinase activation in the tissues of the SN, the expression levels of the reporter gene, *Rosa26-LacZ*, were quantified by immunohistochemistry. The SN was located by counter-staining with tyrosine hydroxylase (TH) to identify dopamine neurons (Fig. 1C). We found that the intensity of LacZ immunofluorescence in the SN was significantly higher in *ndufs4* knockout animals after induction than in wild type littermates (Fig. 1D).

Ndufs4 knockout produced a behavior deficit in the open-field and rotarod tests. PD in humans produces a number of characteristic motor deficits, such as tremor, rigidity, slowness, and postural instability. This motor phenotype is reflected in several rodent models of PD, in the form of decreased latency to fall from an elevated rotating rod (rotarod), and decreased spontaneous activity in an open field, including extending upwards on the hind legs (rearing).

To probe whether the induced *ndufs4* knockout animals experienced motor deficits consistent with PD, we challenged the *ndufs4* knockout and wild type mice to perform the rotarod task. The rotarod is a widely used test to assess behavior deficits in PD rodent models (Meredith and Kang, 2006), and performance on this task has been reported to depend on an intact nigrostriatal dopamine system (M. Angela Cenci, 2005). No decrease in latency to fall was observed in the knockout animals compared with wild type littermates immediately after knockout induction (Fig. 2A; two-way ANOVA, $F_{(1, 100)} = 0.17$, $p = 0.68$), nor at 1 month after induction (Fig. 2A; two-way ANOVA, $F_{(1, 52)} = 0.04$, p

= 0.85). However, at 2 months after knockout induction latency to fall was significantly longer in wild type mice than knockout (Fig. 2A; two-way ANOVA, $F_{(1, 112)} = 10.10$, $p = 0.002$). The difference in latency remained at 3 months after knockout induction (Fig. 2A; two-way ANOVA, $F_{(1, 80)} = 31.89$, $p < 0.0001$), and 5 months after induction (Fig. 2A; two-way ANOVA, $F_{(1, 44)} = 6.29$, $p = 0.016$).

To explore whether this behavior deficit was dopamine-dependent, animals were injected with L-dopa, however this resulted in no improvement in their performance (Fig. 2B). Wild type and induced knockout mice were injected with 25 mg/kg L-dopa following 12.5 mg/kg benserazide, or vehicle control, one hour prior to rotarod testing. Injection with L-dopa did not increase latency to fall in the knockout or wild type mice (Fig. 2B; two-way ANOVA, WT: $F_{(1, 32)} = 2.95$, $p = 0.10$; KO: $F_{(1, 32)} = 1.29$, $p = 0.26$). Each score was then normalized to the same animal's score prior to L-dopa injection, but this also failed to reveal any increase in latency to fall (Fig. 2C; two-way ANOVA, WT: $F_{(1, 32)} = 3.20$, $p = 0.08$; KO: $F_{(1, 32)} = 0.22$, $p = 0.64$). We also observed that the general health of the knockout animals was faltering by 5 months after knockout induction, while the wild type littermates were stable. The body weight of the knockout animals was reduced, as was the quality of their grooming, posture, and attentiveness to being handled (data not shown).

To determine whether *ndufs4* knockout results in a change in spontaneous motor behavior, wild type and knockout mice were allowed to freely explore an open field for 20 minutes while electronic sensors recorded their movements. We found that there was no significant difference in behaviors in the open field immediately or 1 month after knockout induction, but there was a

significant decline in speed, distance, and rearing activity at 2 months after knockout induction (Fig. 3A, B). The reduction in distance and speed traveled also persisted at 3 months after knockout induction (Fig. 3A, data not shown).

Ndufs4 knockout did not result in degeneration of dopaminergic cell bodies in the substantia nigra. If the progressive death of dopaminergic neurons in the SN in PD is due to a deficiency in complex I activity, then we would expect to see a reduction in the surviving number of dopaminergic neurons in the knockout animals compared with their littermate controls. Conversely, if inhibition of complex I function is extraneous to dopamine neuron death, then we would expect to see no reduction in dopamine neuron survival following direct genetic deletion of complex I. To test these two possibilities, we measured the number of TH+ neurons that remained in the SN 3 and 5 months after *ndufs4* knockout induction (Fig. 4A, B). We found that the number of TH+ neurons remaining in the knockout mice was not statistically different from the number found in their wild type littermates (Fig. 4C, D). TH+ cell bodies were counted if they contained an intact nucleus and were located inside the SN. All intact TH+ cell bodies were counted in every 4^{th} coronal section of 30 μm thickness. At both 3 months (Fig. 4C) and 5 months (Fig. 4D) after the induction of the knockout no statistically significant difference was observed in the number of TH+ cell bodies.

Ndufs4 knockout did not result in reduction of TH intensity in the striatum. In PD, the dopamine-releasing axons are believed to degenerate and disappear in advance of the disappearance of their cell somas. Therefore, dopaminergic

fibers may degenerate in the striatum, even though the number of dopaminergic cell bodies in the SN remains unchanged. On the other hand, if the removal of complex I activity does not result in neurodegeneration, we would expect to see no difference in the degree of dopaminergic innervation of the striatum in the knockout animals compared with wild type littermates. To determine if there was any degeneration of dopamine axons in the striatum of *ndufs4* knockout animals we measured the level of intensity produced by TH immunofluorescence. We captured images from normalized locations across the striatum, from animals sacrificed 3 months and 5 months after induction of *ndufs4* knockout using constant imaging parameters and staining conditions. Fluorescence intensity of the striatum was normalized to the background fluorescence of the corpus callosum in the same image. Surprisingly, at 3 months after knockout induction, the knockout mice displayed higher levels of TH+ immunofluorescence in the striatum than their wild type littermates (Fig. 5C). This pattern of increase persisted along the rostrocaudal axis of the striatum (Fig 5D, two-way ANOVA, $F_{(1, 121)} = 26.12$, $p < 0.0001$). For this analysis, we aligned the data taken from each animal using anatomical features, in particular the genu of the corpus callosum, so that the values from each location along the rostrocaudal axis within the striatum could be compared across different animals. At 5 months after knockout induction, there was no longer an increase in TH+ immunofluorescence in the striatum of knockout animals, leaving no difference between the TH+ intensity of the two genotypes (Fig. 6C). The convergence between wild type and knockout TH immunofluorescence intensity at 5 months after knockout induction was persistent along the rostrocaudal axis of the striatum (Fig. 6D).

Ndufs4 knockout resulted in axonopathy of dopaminergic fibers in the striatum. Although the intensity of TH-immunoreactive staining in the striatum was not reduced in the induced *ndufs4* knockout mice, whether the axon fiber structure was intact in the knockout mice remained to be determined. To test the integrity of the axonal branch structure in the striatum we collected images of TH labeled axons using confocal fluorescence microscopy. A series of images was captured from coronal sections spaced at regular 240μm intervals from rostral to caudal (cf. Piggott et al., 1999a; Piggott et al., 1999b; Rea and Simon, 1981), normalized in position to the genu of the corpus callosum. In each coronal section, the image was captured from the center of the striatum of one hemisphere. In these images, the fine axon fiber structure was identified and quantified. We translated each image into a skeletonized graph (Fig. 7A-C; see Methods for details), and used this graph to quantify the number of axonal junctions in a single field, the aggregate length of all the fibers in the field, the average path distance traversed by each individual axon fragment, and the number of axon fragments per field. Using this method, we found that there was no statistical difference in axon structure between the *ndufs4* knockout animals and their wild type littermates at 3 months after knockout induction (Fig. 7D). To confirm this result, a second series of images was captured, from the dorsomedial boundary of the striatum, adjacent to both the lateral ventricle and the corpus callosum. The same imaging and analysis methods were used to quantify these images. Similar to the previously measured location, this dorsomedial location revealed no significant differences between the axon

structures of wild type and knockout animals 3 months after knockout induction (Fig. 7E).

Confocal images were collected and analyzed again at 5 months after knockout induction. At this time point, a significant reduction was observed in the number of junctions, the aggregate length of axon fibers, and the average path length of each sectioned axon fragment in images collected from the central striatum (Fig. 8A). A second image series was also taken from the dorsomedial location of the striatum, and this series showed the same axonal deterioration in the number of junctions, aggregate axon fiber length, and the average path length of individual axon fragments of knockout mice compared with wild type littermates. In addition, a significant difference was seen between genotypes in the number of axon fragments (Fig. 8B). Taken together, these results are consistent with a degeneration of the fine structure of dopamine axons located in the striatum by 5 months after induction of *ndufs4* knockout but not by 3 months.

We next determined whether this axonopathy was distributed uniformly throughout the striatum. We aligned the data taken from each animal to the genu of the corpus callosum, so that the values from each location along the rostrocaudal axis within the striatum could be compared across different animals. In the images from the center of coronal sections of the striatum we observed a larger degree of disparity between knockout and wild type littermates in the rostral end of the striatum (Fig. 8C, E, G). In the images from the dorsomedial boundary of coronal sections of the striatum, we saw a greater significance of degeneration in the caudal end of the structure (Fig. 8D, F, H). However, these

differences are minor, and a significant extent of axonopathy was observed across the entire rostrocaudal axis.

The statistical significance of the rostrocaudal distributions of axon parameters at 5 months after knockout induction were analyzed by two-way ANOVA as follows. At the central location, we observed a significant reduction in junctions (Fig. 8C; two-way ANOVA, $F_{(1, 102)} = 46.97$, $p < 0.0001$), in total length (Fig. 8E; two-way ANOVA, $F_{(1, 102)} = 48.48$, $p < 0.0001$), and in average length of axon fragments (Fig. 8G; two-way ANOVA, $F_{(1, 102)} = 55.87$, $p < 0.0001$). At the dorsomedial location, we observed a significant reduction in junctions (Fig. 8D; two-way ANOVA, $F_{(1, 102)} = 29.69$, $p < 0.0001$), in total length (Fig. 8F; two-way ANOVA, $F_{(1, 102)} = 31.67$, $p < 0.0001$), in the average length (Fig. 8H; two-way ANOVA, $F_{(1, 102)} = 26.30$, $p < 0.0001$), and in the number of axon fragments (data not shown, two-way ANOVA, $F_{(1, 105)} = 12.46$, $p = 0.0006$).

Ndufs4 knockout resulted in axonal spheroids. In the process of analyzing axon structure, we noted that the TH+ axons of the striatum in knockout animals showed the formation of certain enlargements and swellings, referred to as axonal spheroids. Spheroids are an early marker of axon degeneration. Figure 9 shows the morphology of TH immunolabeled axons in the striatum of knockout mice (Fig. 9B) and their wild type littermates (Fig. 9A). As seen in these representative images, the knockout is replete with axonal spheroids while the wild type has nearly none. The occurrence of spheroids was quantified in both wild type and knockout tissues, by an experimenter blind to genotype, and we observed a striking increase in the number of spheroids in the TH+ axons of

knockout animals compared with wild type littermates, both at 3 months (Fig. 9C) and at 5 months (Fig. 9D) after induction.

To determine if the spatial distribution of these spheroids was focal or generalized, we analyzed the distribution of spheroids along the rostrocaudal axis of the striatum. We observed that spheroid formation was elevated along the entire length of the central striatum at 3 months (Fig. 10A) and 5 months (Fig. 10C) after induction of the *ndufs4* knockout. In the dorsomedial striatum, the spheroids were also significantly elevated along the entire rostrocaudal axis, with additional concentration near the midpoint along the axis, both at 3 months (Fig. 10B) and 5 months (Fig. 10D) after knockout induction.

The appearance of these spheroids at 3 months after induction, before a deterioration of axon fibers is observed, provides an explanation for some of the earlier data we collected. Spheroids appear to be wider and emit more immunofluorescence than ordinary axon fibers of the same length. If spheroids form prior to a decrease in axonal arbor complexity, then they could be expected to augment the baseline level of immunofluorescence intensity, similar to the result we recorded in the tissues from 3 months after knockout induction (Fig. 5C, D), even though the axon structure appeared unchanged as measured by the skeletonization assay (Fig. 7D, E). Furthermore, if spheroids persist or accelerate after a decrease in axonal arbor complexity, then the fluorescence intensity they contribute could compensate for that intensity lost as ordinary axon fibers degenerate, with the result that the aggregate fluorescence intensity appears unchanged, similar to the result we recorded in the tissues from 5 months after knockout induction (Fig. 6C, D), even though the axon structure

appeared to be significantly reduced as measured by the skeletonization assay (Fig. 8).

Mitochondrial morphology was altered in dopamine neurons from ndufs4 knockout SN. Mitochondrial dynamics have been shown to be disrupted in animal or cell culture models of several Parkinson-causing genes including PINK1, DJ-1 and parkin (Lutz et al., 2009; Wang et al., 2012). Changes in mitochondrial dynamics have additionally been reported after rotenone treatment, which is another PD model (Barsoum et al., 2006; Benard et al., 2007). As a mitochondrial protein, NDUFS4 also has the potential to interfere with the shape or dynamics of the mitochondria directly, regardless of disease relevance. To assess whether mitochondria in the dopaminergic neurons were structurally affected by the loss of *ndufs4*, we used an antibody against the mitochondrial marker protein Tom20 to visualize the mitochondria in TH+ neurons. We compared the total Tom20 immunofluorescence intensity of each cell, and observed no difference between the cells taken from knockout and wild type animals at 3 months after knockout induction, whether measured directly or normalized for the volume of the cell body (Fig. 11A). However at 5 months after knockout induction, we did observe a significant decrease in Tom20 staining intensity in the cells imaged from knockout animals (Fig. 11B).

To compare the mitochondrial structure between genotypes, we measured their size, length and count using two quantitative techniques (see Methods for details), a skeletonization model (Fig. 12A-C) and a space-filling model (Fig. 13A-C). Using the skeletonization model, we observed no difference in total length of

mitochondria in the TH+ cells of knockout animals compared with wild type littermates. However, we did observe a significant decrease in average length at both 3 months (Fig. 12D) and 5 months (Fig. 12E) after knockout induction. We recorded no difference in the count of mitochondrial particles at 3 months after knockout induction (Fig. 12D), but we did detect a significant increase in the count at 5 months after induction (Fig. 12E). Increases in count and decreases in average length suggest a shift towards fission or fragmentation of mitochondria.

Using the space-filling model, we observed no change in the count or aggregate volume of mitochondrial particles at 3 months (Fig. 13D) or 5 months (Fig. 13E) after knockout induction. However, we did observe a significant decrease in average volume of mitochondrial particles in TH+ cells from *ndufs4* knockout animals, at 5 months (Fig. 13E) but not 3 months (Fig. 13D) after knockout induction, compared with the mitochondria of TH+ cells from wild type littermates. This decrease is consistent with the results we collected from the skeleton assay, indicating that the average mitochondrial particles from 5 months after knockout induction seem to be both shorter length and smaller volume than the mitochondria of wild type littermates.

Chapter3

DISCUSSION

Numerous lines of evidence have suggested that interference with mitochondrial complex I constitutes the impetus of PD pathogenesis. First, evidence of reduced complex I activity was found in the post-mortem tissues of human patients with PD (Keeney et al., 2006; Mizuno et al., 1989; Parker et al., 1989). Second, two chemically diverse complex I inhibitors, MPTP and rotenone, have long been used to recapitulate the phenotype of PD in animal models (Dauer and Przedborski, 2003). And furthermore these animal models can be rescued by over-expressing the yeast complex I analog NDI1 (Barber-Singh et al., 2009; Marella et al., 2008), which is rotenone- and MPTP-insensitive.

However, these reports do not exclude the possibility that complex I inhibition is a consequence of disease pathology, and not itself the cause. Alternative explanations for the toxicity of both rotenone and MPTP have been proposed. Rotenone is a potent destabilizer of microtubules (Choi et al., 2011; Marshall and Himes, 1978), and rotenone and MPTP both cause increases in oxidative stress (Cleeter et al., 1992; Li et al., 2003). The yeast NADH dehydrogenase NDI1, which has been used to rescue rotenone and MPTP, also reduces the amount of oxidative damage (Marella et al., 2008). The observation that NDI1 expression protects against rotenone or MPTP is consistent with the hypothesis that oxidative stress, not the loss of complex I activity, is the mechanism of selective dopaminergic neurodegeneration. As the authors note, “these observations provide further support for the hypothesis that oxidative damage is the primary mechanism by which complex I inhibitors cause toxicity”

(Sherer et al., 2007). If complex I inhibition causes oxidative damage, and oxidative damage causes complex I inhibition (Cleeter et al., 1992), then separating cause from effect will be extremely difficult, and it prevents us from concluding that complex I inhibition *per se* is necessary or sufficient for dopamine degeneration in this model.

NDI1 protection can also be mediated by elevating ATP levels, or reducing NADH levels. ATP and other intracellular nucleotides can act as pro-survival factors, by binding to cytochrome C and inhibiting apoptosome formation (Chandra et al., 2006). High levels of NADH have been shown to stimulate endogenous dopamine biosynthesis, by enhancing the level of H4Biopterin, a co-factor of TH (Vrecko et al., 1997). This has even been used to raise dopamine levels in PD patients (Kuhn et al., 1996). Elevated dopamine biosynthesis could result in dopamine auto-oxidation and cytotoxicity (Hastings et al., 1996). This has been proposed to mediate the selective vulnerability of dopamine neurons in PD (Miyazaki and Asanuma, 2008). Therefore simply by metabolizing its substrate, an NADH dehydrogenase can reduce the risk to dopamine neurons of oxidative stress.

Time course of neurodegeneration in ndufs4 knockout model

In this study we sought to answer the question of whether the loss of complex I activity causes dopaminergic neurodegeneration. By inducing the knockout in mature, adult mice, we were able to monitor the effects of the loss of complex I activity on dopamine neurons in their native milieu over the course of 5 months. The fact that we did not see any reduction in the number of surviving

TH+ neurons following genetic deletion of complex I suggests that lack of complex I activity is not sufficient to explain the dopaminergic cell death in PD. This agrees with previous findings in dissociated primary dopaminergic neuron culture (Choi et al., 2008). The toxicant models of complex I inhibition take effect on a much shorter timescale than 5 months. MPTP's effect is immediate in mice and both human and non-human primates. Even gradual application of MPTP only required 1 month to observe PD-like symptoms (Fornai et al., 2005). Similarly, the rotenone model of PD in rats and mice takes only 1 month before neurodegeneration is apparent (Betarbet et al., 2000; Inden et al., 2007). In the present study, the absence of cell death after 5 months suggests that it is not forthcoming, however the possibility remains that at longer time points, dopaminergic neurodegeneration might have been observed in the *ndufs4* knockout.

The ability of adult mice lacking *ndufs4* to survive for 5 months after knockout induction may be due to compensatory mechanisms. The conventional *ndufs4* knockout mouse was found to have an elevation in the level of complex II activity (Kruse et al., 2008), which like complex I transports electrons to ubiquinone, and like NDI1 it does not translocate protons across the mitochondrial inner membrane. It was hypothesized that the energy demands of the developing brain might accelerate the damage caused by insufficient oxidative phosphorylation (Kruse et al., 2008), which is consistent with the observation that the duration of viability is longer when *ndufs4* knockout is induced in adulthood. Other possible compensatory mechanisms were identified in a *Drosophila* model of nearly complete loss of ATP synthase activity. It was

found that this mutant strain compensated for the lack of oxidative phosphorylation by increasing glycolysis, ketogenesis, and Kreb's cycle activity (Celotto et al., 2011).

Implications of motor deficits

We observed a motor deficit on the rotarod test, however this phenotype did not seem to be specific to the dopamine system because it was not ameliorated by injection of L-dopa, the dopamine precursor. Because we found a significant deterioration of the dopamine axons in the striatum, the lack of a motor improvement after L-dopa injection is likely due to either (1) a failure to metabolize L-dopa to dopamine by dopa decarboxylase, or (2) the damage of other neuron types necessary for normal motor performance in the induced *ndufs4* knockout mice. This second reason is likely, due to a recent finding that the conventional *ndufs4* knockout mouse experiences severe respiratory defects, and that *ndufs4* deletion in the vestibular nuclei of the brainstem was both necessary and sufficient to produce this phenotype (Quintana et al., 2012). It is plausible that the same brain regions would be vulnerable to *ndufs4* knockout induced at adulthood, and that they would be required to perform the rotarod task.

Axonal degeneration and spheroids

In this study, we observed axonopathies in the striatum of *ndufs4* knockout mice 5 months after knockout induction resembling axonal fragmentation, retraction, and the formation of axonal spheroids. These axonal spheroids were consistent with those observed in the dystrophic striatal axons of

mice transgenically expressing the PD-linked R1441G mutation of LRRK2 (Li et al., 2009b). Similar to our findings, these transgenic LRRK2 mice showed no reduction in total TH expression in the striatum, despite axonal dystrophy and behavioral deficits (Li et al., 2009b). Other pathogenic LRRK2 mutations G2019S and I2020T were also shown to result in spheroid inclusions, as well as a significant reduction of neurite length and arbor complexity in cultured rat cortical neurons after transfection (MacLeod et al., 2006), and cultured transgenic mouse dopamine neurons (Ramonet et al., 2012) and hippocampal neurons (Parisiadou et al., 2009). Axon degeneration has been reported in other PD models as well. After MPTP more reduction was seen in the dopaminergic axon fibers in the medial forebrain bundle than in the dopaminergic cell bodies in the SN of the same animals (Li et al., 2009a). And in cultured dopaminergic neurons, it was reported that MPP+ treatment resulted in microtubule destabilization and a shortening of neurites and a beading morphology due to impaired axonal transport (Li et al., 2009a). These reports suggest that the axonal dystrophy, both spheroids and reduction in axon length and complexity, which we observed in *ndufs4* knockout animals 5 months after knockout induction, is consistent with the structural axon defects resulting from the PD-causing mutations in the LRRK2 gene and the PD toxicant model MPTP.

Axonal spheroids were also described in the brains of patients with PD and Dementia with Lewy Bodies (DLB), in the hippocampus but not in the striatum (Galvin et al., 1999). Similar axonal morphologies have also been observed in mouse models of Alzheimer's disease (Tsai et al., 2004), Huntington's disease (Li et al., 2001), and also human Alzheimer brains (Stokin

et al., 2005), human Creutzfeld-Jacob disease brains (Liberski and Budka, 1999), human HIV dementia brains (Adle-Biassette et al., 1999), human multiple sclerosis brains (Ferguson et al., 1997; Trapp et al., 1998), and models of traumatic brain injury (Cheng and Povlishock, 1988) and axotomy and 6-OHDA lesion (Cheng et al., 2011).

The axonal spheroids which we observed in *ndufs4* knockout mice were visible earlier in the experimental time-course than the disappearance of TH+ axon fibers. This sequence suggests that the axonal dystrophy began early on, and is consistent with other reports of axonal spheroids, which appear preceding axon fragmentation (Coleman, 2005). This could provide a promising avenue to measure the effectiveness of future experimental interventions to elucidate or prevent the axonal degeneration due to *ndufs4* knockout, or possibly other complex I inhibition models. Further study will be required to determine if this axon degeneration or spheroid formation is specific to dopamine neurons. If other neuron types are also affected then spheroid formation may precede the degeneration of axons in those cells as well.

It has been reported that the arborizations from individual SN neurons are dense, widespread, and greatly overlap each other, with the breadth of a single arbor spanning about 3% of the volume of the striatum (Matsuda et al., 2009). It is mainly for this reason that visually extricating a single neuronal arbor from its neighbors is extremely difficult without using exogenous cell tracers prior to death. We decided to simply treat each axon fragment contained within the sectioned tissue equally, regardless of whether they originate from the same or different

neurons in the SN. With enough samples, this strategy should allow us to arrive at the same result as the examination of individual axonal arbors.

Degree of axon degeneration compared with loss of cell bodies in PD

It is difficult to know what degree of dopamine axon or cell body degeneration constitutes a similarity with that seen in PD. One widely repeated figure is at the time of symptom onset the PD patient has already lost 80% of the dopaminergic terminals in the striatum and upwards of 50-60% of the dopaminergic cell bodies in the SN (Alberio et al., 2012; Dauer and Przedborski, 2003; Matsuda et al., 2009; Stoessl et al., 2011). This figure could be related to a report by Fearnley and Lees who observed in 1991 that out of six subdivisions of the human SN, the lateral ventral tier showed the greatest degree of cell loss at 68% decrease (Fearnley and Lees, 1991). However this was the most severely affected segment of the SN, and their estimate of the number of neurons lost in the entire SN at the time of onset was only 30%. Another estimate of neuron loss at time of onset reported a 29% reduction (Greffard et al., 2006). These studies used linear or logarithmic regression from the remaining neurons at time of death, to project backward to the time of symptom onset. Other studies use regression to estimate the dopamine content in the striatum, rather than cell bodies in the SN. They report that reduction of dopamine at disease onset was calculated to be 68% and 82% for patients with disease onset at age 60 and 73 respectively (Riederer and Wuketich, 1976)By measuring the relative level of vesicular monoamine transporter 2 (VMAT2) activity as a marker for the extent of dopaminergic innervation at time of death, rather than dopamine

content, it was calculated that about 50% reduction in VMAT2 innervation correlated with disease onset, regardless of age (Scherman et al., 1989). Finally the relative activity of dopamine terminals can be measured in living patients *in vivo* using radio-labeled substrates. This also allows us to distinguish, in patients who display symptoms unilaterally, the difference in lesion between the symptomatic and asymptomatic sides, likely representing the window within which the degree of dopamine loss transitions from benign to pathological. By use of this method it was observed that the difference between the symptomatic and asymptomatic sides of unilateral PD patients lies somewhere between 38-53% reduction in dopamine and 51-62% reduction in VMAT2 (Lee et al., 2000). In total, these findings are consistent with the hypothesis that degeneration of axons in PD occurs prior to, or at least in greater proportion to, the degeneration of the neuron soma in the SN. Furthermore the estimates of axon function in PD vary widely, and some parameters of axon function might be reduced by as little as 40% (Lee et al., 2000). Therefore it is possible that the proportion of axon degeneration we observed might be consistent with the degeneration of PD at the time of symptom onset, and thereby contribute to disease even if it fails to elicit any degeneration of nigral cell bodies. Further investigation of the functional consequences of this degeneration would be needed to answer this question.

Shift in mitochondrial size in ndufs4 knockout

We observed a small but significant reduction in the average size of mitochondrial particles within the dopaminergic neurons of *ndufs4* knockout mice

compared to their wild type littermates. This difference is consistent with a shift in the balance of mitochondrial dynamics towards greater fission or a reduction in fusion. It was recently shown that loss of the AR-JP genes parkin or PINK1 result in an increase in mitochondrial fission in human dopaminergic SH-SY5Y cells (Lutz et al., 2009), and that in cultured mouse hippocampal neurons, PINK1 knock-down produced a shortening of the average mitochondrial particle length by 18% in the soma and 12% in the processes (Lutz et al., 2009). Our result supports a shift in the balance of mitochondrial dynamics away from fusion, which would be consistent with the PINK1/parkin model in which PINK1 accumulates on depolarized mitochondria and recruits parkin to mediate their clearance by way of disabling mitochondrial fusion (Pallanck, 2010). If *ndufs4* knockout causes a reduction in mitochondrial membrane potential, then this model predicts that PINK1 would recruit parkin to these mitochondria and facilitate their degradation. A competing model has also been proposed, in which PINK1 knockout actually causes a reduction in mitochondrial membrane potential, by itself inhibiting complex I (Morais et al., 2009), although another study found that genetic silencing of PINK1 had a larger effect on complex IV activity than on complex I (Gegg et al., 2009). This model also predicts that parkin will segregate depolarized mitochondria by disabling fusion. Both models of the role of the PD-related protein parkin in mitochondrial dynamics are consistent with the results we observed. Future studies could test the role of parkin in regulating mitochondrial size in the *ndufs4* knockout by measuring changes in parkin localization, or by testing if the changes in mitochondrial size are dependent on parkin expression.

Our results are also consistent with reports from studies of complex I deficiency in human patients. Using fibroblasts cultured from patients with complex I mutations, the structure of mitochondria was reported to be significantly effected, in a trend consistent with mitochondrial fission (Koopman et al., 2005). Primary fibroblast cell lines were derived from 13 patients with isolated complex I deficiencies including 4 with *ndufs4* mutations, 8 with other complex I gene mutations, one patient with no known mutation, and 4 control patient cell lines. Researchers found a small reduction in the average length of mitochondria and an increase in count of mitochondria, in many of the patient cell lines (Koopman et al., 2005). Furthermore, this phenotype was rescued by fusing the cells from two patients with mutations in different genes, *ndufs1* and *ndufs2* (Koopman et al., 2005). This restoration was attributed to complementation between the un-mutated gene from each cell, identifying the mutations as the cause of the morphological changes. This report suggests that our mitochondrial results might be shared across species and cell types. Furthermore, the report of reversal upon complementation suggests that the change in size we demonstrated might be a result of complex I deficiency, not an indirect reaction to axon degeneration or other neuron-specific challenges.

Chapter 4

FUTURE DIRECTIONS

In this study we discovered distinct axonopathies occurring long after the induction of *ndufs4* knockout. This long delay makes experiment design difficult, however it does recapitulate the extremely long time-course of disease pathogenesis believed to take place in human sporadic PD. Prior to this work, our lab had shown that *ndufs4* knockout caused no deleterious effect on the survival of dopamine neurons in culture (Choi et al., 2008; Choi et al., 2011), but it was not known whether *ndufs4* knockout recapitulated any PD-related characteristics, cell death notwithstanding. Now that we have shown that *ndufs4* knockout results in clear axonal dystrophy in dopaminergic neurons, it will be interesting to investigate whether and to what degree this pathology is selective to dopaminergic neurons over other neuronal types.

In future experiments, it will also be of interest to observe how far the observed axonopathy progresses. Unfortunately, in the inducible model used for this study, no further progression was possible due to the flagging health of the animal subjects. The induced knockout was not restricted to the brain, and while subjects lived for far longer than the 50 day lifespan of the conventional *ndufs4* knockout, their body weight and other signs of general welfare were falling at the time the experiment ended. Indeed, the planned experimental time-course of 6 months needed to be abbreviated to 5 months for this reason. It was recently discovered that the lifespan of the conventional *ndufs4* knockout mouse can be extended by viral re-expression of *ndufs4* in the vestibular nuclei (Quintana et al., 2012). The vestibular nuclei play a role in regulation of breathing (Hernandez et

al., 2004), and the conventional *ndufs4* knockout mice showed breathing irregularities (Quintana et al., 2010; Quintana et al., 2012), so this may have contributed to the behavior deficits we observed in the inducible *ndufs4* knockout animals, as well as to the deterioration of their overall health. Viral Cre expression in the SN could provide a knockout of *ndufs4* in all the cell types in the region, both neuronal and glial, without incurring the shortened lifespan which seems to be related to the vestibular nuclei. The conditional *ndufs4* knockout restricted to dopamine neurons using the dopamine transporter promoter (DAT-Cre) remains healthy for over 2 years (Sterky et al., 2011). Therefore, if similar axonopathies are observed in the striatum of any of these *ndufs4* knockout models, then study of further progression of the condition would be achievable.

Using any SN-specific induction also includes another experimental advantage in that the dopaminergic axons express a marker protein produced by the floxed-stop *Rosa26-LacZ* reporter gene. This will hopefully make it possible to measure the degeneration of dopaminergic axons irrespective of TH protein expression. It has been reported that dopaminergic axons cease expression of TH prior to retraction or degradation, making them difficult to visualize accurately (Cheng et al., 2011). However, ectopically expressed marker proteins are often not subject to this limitation (Cheng et al., 2011). Wild type littermates do not express the marker, which would interfere with using the same marker to measure both wild type and knockout tissues. However it has been reported that the loss of TH expression in surviving former dopaminergic neurons accounts for only 3% of neurons in wild type or vehicle controls (Baquet et al., 2009), while the inactivation of TH expression in disease model conditions like MPTP can be

much higher (Ozaki et al., 1988). This suggests that the reporter gene is only needed in the knockout animals, while in wild type the reporter and endogenous markers (e.g. TH) will be nearly redundant. This could easily be confirmed by using *Ndufs4/Rosa26-LacZ* heterozygotes expressing Cre in the control group. *Ndufs4* heterozygotes were reported to be indistinguishable from wild type (Choi et al., 2008; Kruse et al., 2008), suggesting *ndufs4* haplo-sufficiency and therefore the heterozygote can be used for control.

Our observations of the reduction in mitochondria size and volume 5 months after knockout induction were consistent with a trend towards fragmentation or fission. It has been proposed that mitochondrial dynamics in a healthy neuron help support normal axonal transport (Saxton and Hollenbeck, 2012), and that SN neurons' extensive transport requirements and distant axon terminals might contribute to their selective vulnerability to alterations of mitochondrial dynamics in PD. Therefore it will be interesting to examine whether transport of mitochondria to the axon terminals is disrupted in the *ndufs4* knockout, and indeed whether the levels of axon transport correlate with mitochondrial fragmentation in the somas of the same animals. Axonal spheroid formation accompanying axon damage or fragmentation has also been attributed to defects in axon transport (Coleman, 2005), although other potential causes have also been proposed. It will be interesting to see whether the widespread increase in axonal spheroids that we observed is accompanied by defects in axonal transport, or is related to mitochondrial fission or ATP production. The mitochondrial fission protein DRP1 can be inhibited *in vivo* by conditional knockout (Kageyama et al., 2012) or by systemic injection of DRP1 inhibitors

(Grohm et al., 2012), that could be used to test whether fission is necessary for the observed axonal degeneration. Conversely, viral over-expression of DRP1 could determine whether increase in fission is sufficient to produce axonopathy. Finally, tracing individual axons with dyes or exogenous markers (Matsuda et al., 2009) could reveal if fragmented mitochondria correlate with axon degeneration within the same neuron.

Chapter 5

METHODS

Animals. All animal experiments were performed with the approval of the Institutional Animal Care and Use Committee of the University of Washington. Mice were maintained on rodent diet (5053, PicoLab) and water available *ad libitum* in a vivarium with a 12 hr light/dark cycle at 22°C. Generation of *ndufs4*$^{lox/lox}$ *Cre-ER*^{t2} mice has been described (Quintana et al., 2010). At 12 weeks of age, both Cre and non-Cre male animals were orally administered freshly dissolved Tamoxifen (Sigma) at a dose of 250 mg/kg body weight dissolved in corn oil (Sigma) and 2% acetic acid (VWR), once daily for 10 days. Tamoxifen administration was halted when body weights dropped to 85% of starting weight, and resumed when weights rebounded (2 weeks later). Therefore, the dosing schedule used was 8 consecutive days, followed by 2 more consecutive days, 2 weeks later.

Behavior, open field. Mice were placed gently into the center of a 10cm x 10cm chamber and allowed to move freely for 20 minutes. The x, y and z coordinates were measured by infrared beams using TruScan software (Coulbourn Instruments).

Behavior, rotarod. Mice were placed gently on an elevated rotating rod device (San Diego Instruments) 4 mice at once, in isolated enclosed lanes. The rod was elevated 1 foot above a 1-inch layer of foam. For training, the rod was turned at a constant speed of 4 rpm. This training lasted until all 4 mice were able to remain on the rod without falling for 60 seconds. For testing, the rod accelerated

steadily from 0 rpm to 40 rpm at a steady increase over 300 seconds. Infrared beams electronically recorded the time and distance traveled by each mouse before falling. Mice were allowed between 60 and 300 seconds between trials. Eight consecutive trials were recorded from each mouse, and the last 4 trials were used for data analysis.

L-Dopa injection. All drugs were freshly dissolved in isostatic saline. Mice were IP injected with benserazide (Fisher) at 12.5 mg/kg body weight, followed twenty minutes later by IP injection with L-dopa (Fisher) at 25 mg/kg body weight. After 60 minutes mice were administered the rotarod test as described.

Western Analysis. Freshly extracted brain tissues were mechanically homogenized and prepared as described (Derijard et al., 1994).

Complex I Activity Assay. Mitochondria were isolated as described (Tieu et al., 2003). Isolated mitochondria were assayed for oxygen consumption by polarography as described (Tieu et al., 2003).

Immunohistochemistry. Mice were transcardially perfused with ice cold phosphate buffered saline (PBS) followed by 4% paraformaldehyde (PFA) in PBS. Brains were extracted and incubated in 4% PFA overnight, then in 30% sucrose in PBS until saturated, then frozen on dry ice. Coronal sections of 30 μm thickness were collected on slides using a Leica cryostat and stored at -20 C. Tissues were permeabilized in 1% triton X-100 (Sigma) and 10% normal goat serum (Gibco) or donkey serum (Sigma) for 1 hour prior to primary antibody incubation in 0.25% triton X-100 and 10% normal goat serum for 2 days at 4 C. Slides were incubated in secondary antibody (Invitrogen) for 4 hours at room temperature. Hoechst 33342 (Invitrogen) was applied for 15 minutes. For

mitochondrial imaging, hydrophobic barrier applied for staining was removed using xylenes, and precision-thickness coverslips (Deckgläser) were used for mounting. Aqua-Polymount was used for all slides. Primary antibodies used were rabbit anti-TH (1:2000, Pel-Freez), rabbit anti-Tom20 (1:100, Santa Cruz), sheep anti-TH (1:500, Millipore), mouse anti-β-gal (1:1000, Promega), and mouse anti-MAP2 (1:1000, Sigma).

Axon structure analysis. One in every eight 30μm coronal sections of the striatum was captured by Olympus Fluoview-1000 laser scanning confocal microscope. Image stack was captured using 60x oil immersion lens, 1x zoom, 3 optical slices with 0.47μm step size, 1024x1024 pixels. This 3D image was analyzed in a script developed for this purpose (Fig A1), executed in the FIJI (Fiji Is Just ImageJ) distribution of the ImageJ software (NIH). The method of analysis began with the Tubeness plug-in (Sato et al., 1998), which detects directionality in the image irrespective of gain. The output of the tubeness plugin was thresholded to a 2 bit image, which was converted to a skeletonized graph using the Skeletonize plug-in (Arganda-Carreras et al., 2010). Finally, the Analyze Skeleton plug-in produced the numbers of junctions, paths, and lengths contained in the skeleton (Arganda-Carreras et al., 2010). The number of “slab voxels” was used to compare total length, and the “longest shortest path” was used to compare average length.

Mitochondria structure analysis. Confocal images of individual cells immunopositive for both TH and LacZ were captured using 100x oil immersion lens, 4x zoom, 30 optical slices with 0.100 μm step size, 640x640 pixels. This 3D image was subjected to deconvolution using Huygens Professional software,

with signal to noise ratio of 40 (empirically derived using Tom20 immunostaining). The deconvolved image was analyzed in a script developed for this purpose (Fig A2), executed in FIJI (ImageJ). Briefly, the TH channel was used to mask a region of interest in the Tom20 channel. The 3D Object Counter plugin was used to produce the measures of count and volume, and then the tubeness and skeletonize plugins were used as above to produce a measure of length ("longest shortest path").

Statistical Evaluations. Comparisons were made using one-way ANOVA or two-way ANOVA for repeated measures. Statistical significance was achieved when $p < 0.05$ (*), $p < 0.01$ (**), $p < 0.001$ (***). All error bars represent S.E.M.

FIGURES

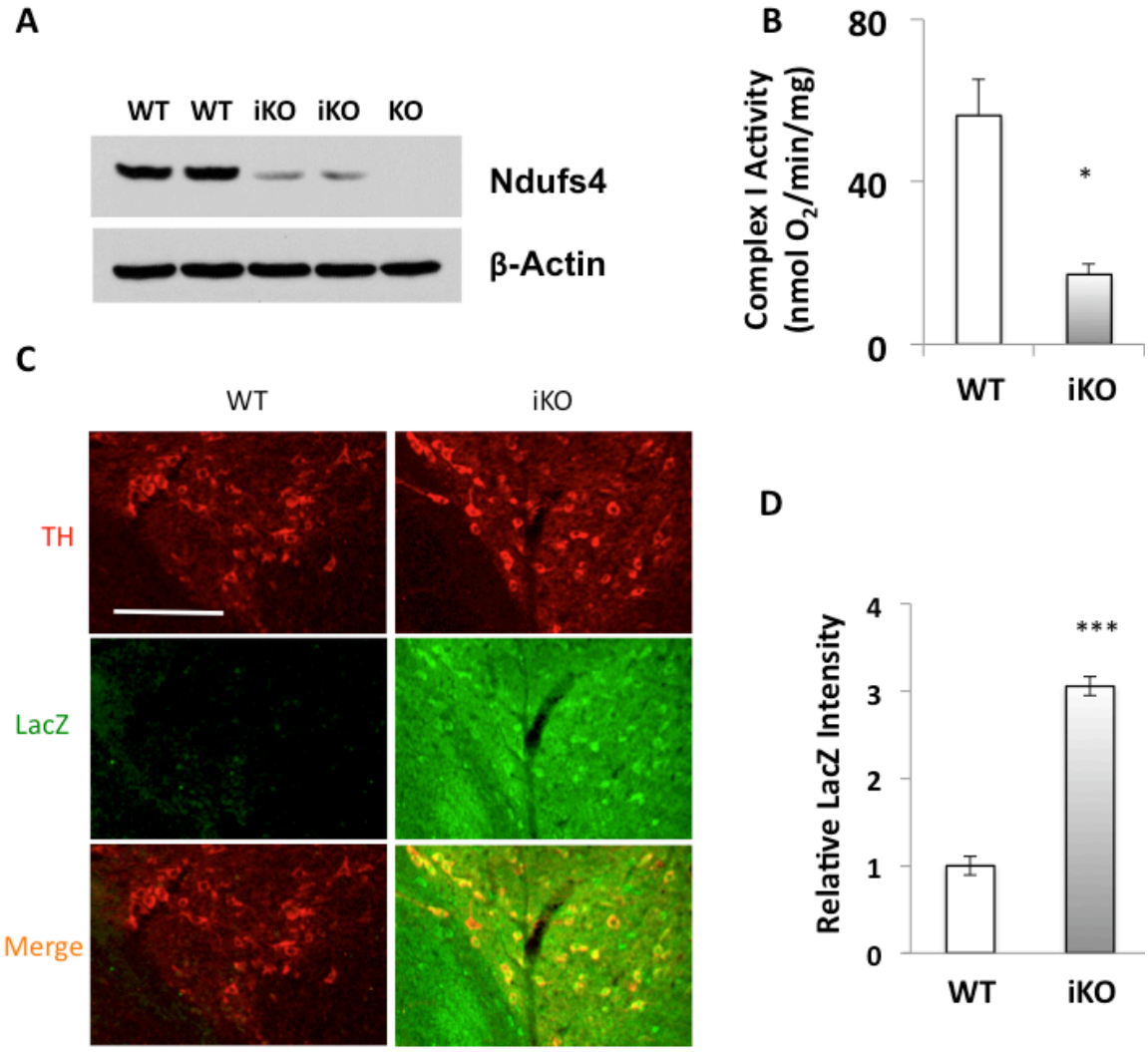

Figure 1. Verification of the induced knockout.

(A) NDUFS4 protein expression in the brain was measured by western blot. (B) The oxygen consumption rate of purified mitochondria from the brain was measured by polarography. The rate before and after addition of rotenone was compared to isolate complex I dependent oxygen consumption. The complex I dependent oxygen consumption was significantly lower in knockout mitochondria (filled bar) compared with wild type (open bar). (C) Representative images showing Rosa26-LacZ (green) reporter protein immunostaining in the SN. The SN was located by TH immunostaining (red). Scale bar: 100 µm. (D) Quantification of the intensity of LacZ immunostaining in the SN from *ndufs4* knockout animals (filled bar) compared with wild type littermates (open bar). Abbreviations: WT, wild type; iKO, induced knockout; TH, tyrosine hydroxylase;

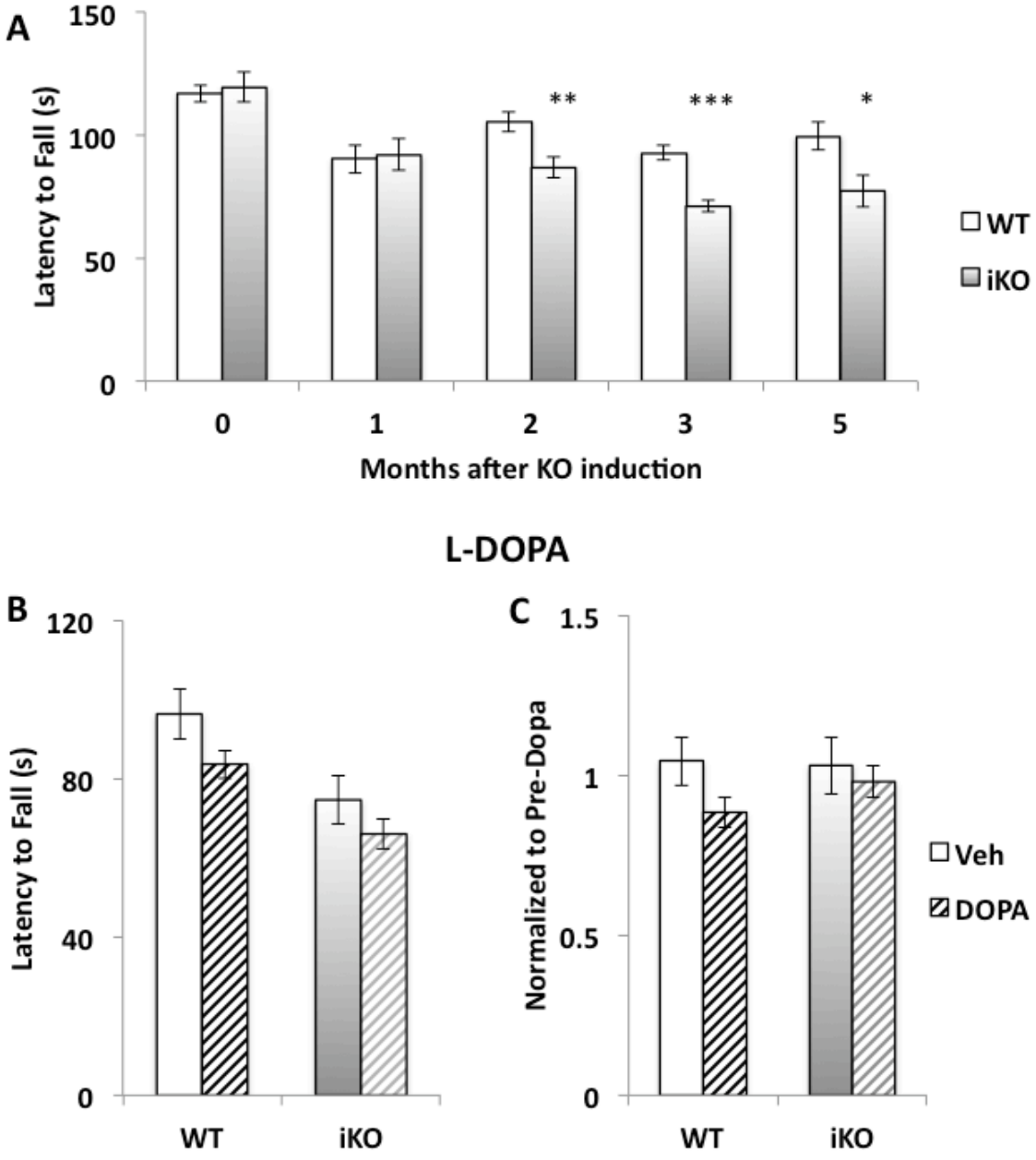

Figure 2. *Ndufs4* knockout mice were impaired on the rotarod.

(A) The latency of mice to fall off the rotarod was tested in 4 consecutive trials, at 5 time points after knockout induction. At 2 months or more after knockout induction, the latency to fall was significantly shorter in knockout animals (filled bars) compared to wild type littermates (open bars). (B) Mice were re-tested after injection of L-dopa, at 3 months after knockout induction. No rescue of motor behavior was seen after L-dopa injection (hashed bars) compared with vehicle injection (smooth bars). (C) The rotarod scores from B were normalized for each animal's pre-dopa score.

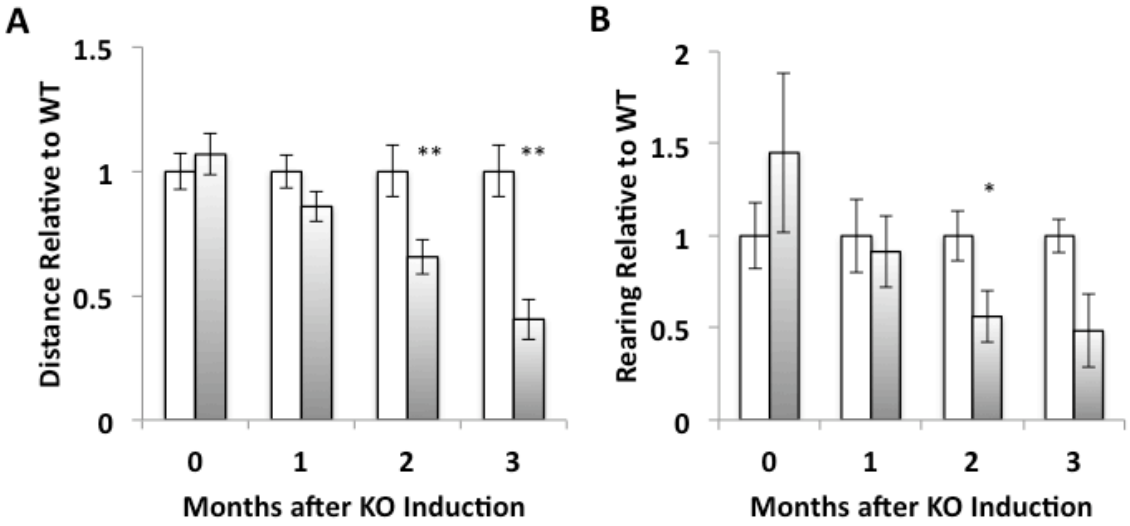

Figure 3. Spontaneous activity in the open field.

(A) At 2 months or more after knockout induction, distance traveled was significantly shorter by *ndufs4* knockout mice (filled bars) compared with wild type littermates (open bars). (B) The time spent in the vertical plane (rearing) was significantly less in knockout animals (filled bars) compared with wild type (open bars), at 2 months after knockout induction. But the difference at 3 months was not significant.

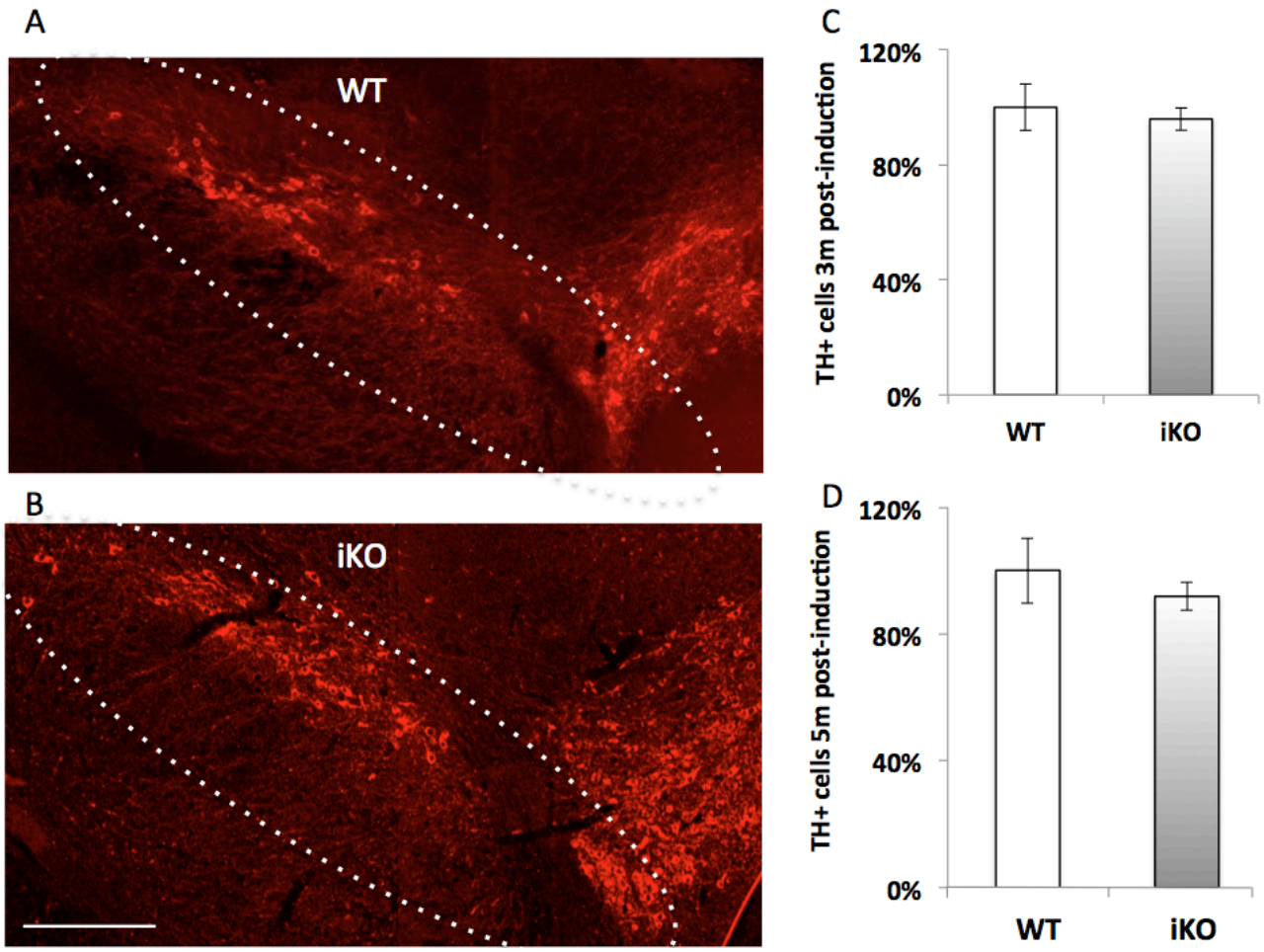

Figure 4. The number of remaining TH+ neurons in the SN was not reduced in *ndufs4* knockout.

(A, B) Representative images showing TH+ cell bodies in wild type (A) and knockout (B) SN tissues. The white line indicates the location of the SN. Scale bar: 250 μm for A, B. (C, D) The number of remaining TH+ cell bodies with intact nucleus in the SN was quantified at 3 months (C) and 5 months (D) after knockout induction. The SN was quantified from very fourth coronal 30 μm section along the entire rostrocaudal length of the SN. The difference in survival number between knockout (filled bars) and wild type (open bars) was not significant at either time point, by one-way ANOVA.

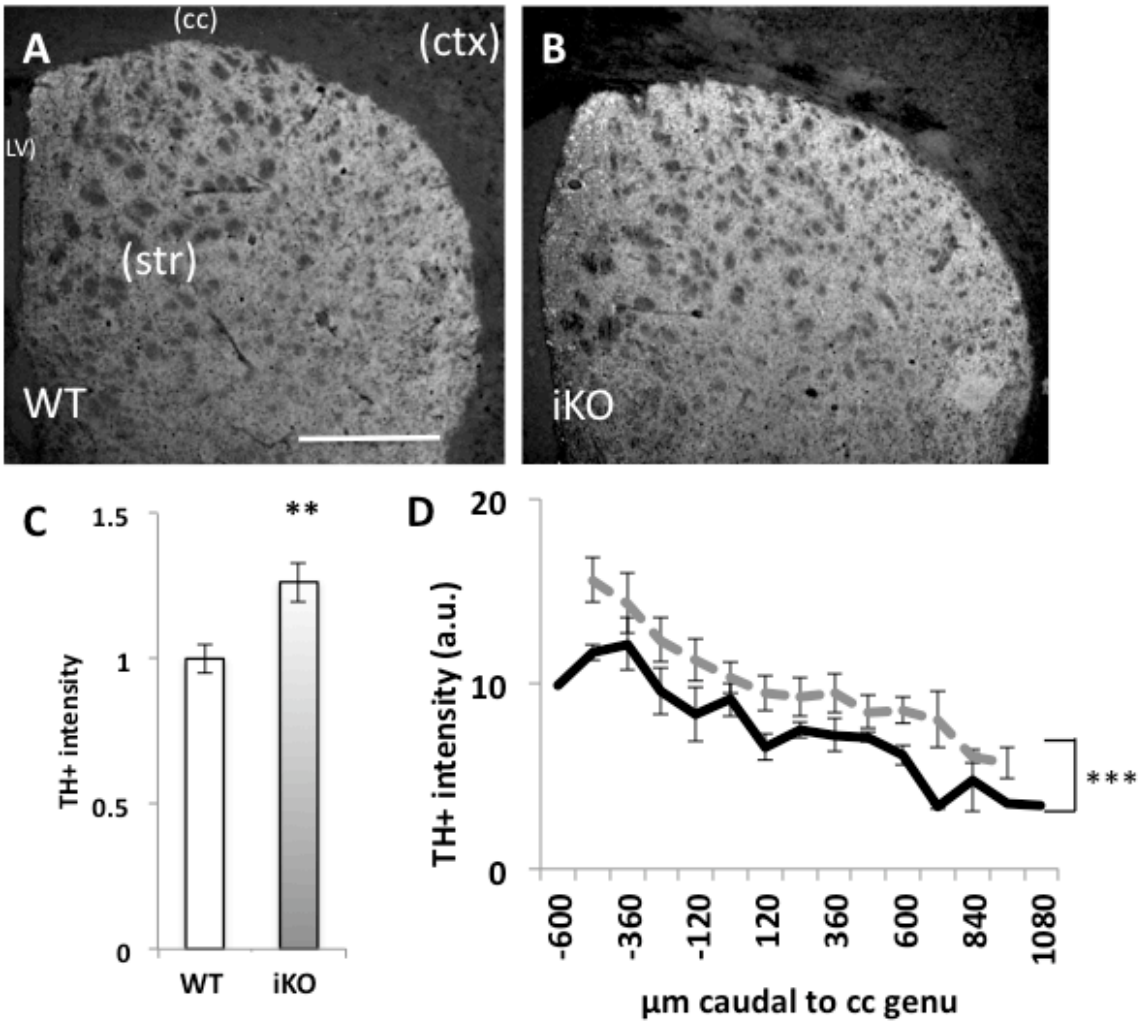

Figure 5. TH+ staining intensity of dopaminergic innervation in the striatum was increased after 3 months.

(A, B) Representative images of TH+ immunostaining in striatum of wild type (A) and induced *ndufs4* knockout (B) animals 3 months after knockout induction. Scale bar: 250 µm for A, B. (C) Quantification of TH immunofluorescence intensity in wild type (open bar) and induced knockout (filled bar) striatum. (D) Quantification of the pattern of TH immunofluorescence of wild type (solid line) and induced knockout mice (dashed line) along the rostrocaudal axis of the striatum. Striatal sections were normalized to the genu of the corpus callosum. Abbreviations: str, striatum; cc, corpus callosum; lv, lateral ventricle; ctx, cortex; a.u., arbitrary units.

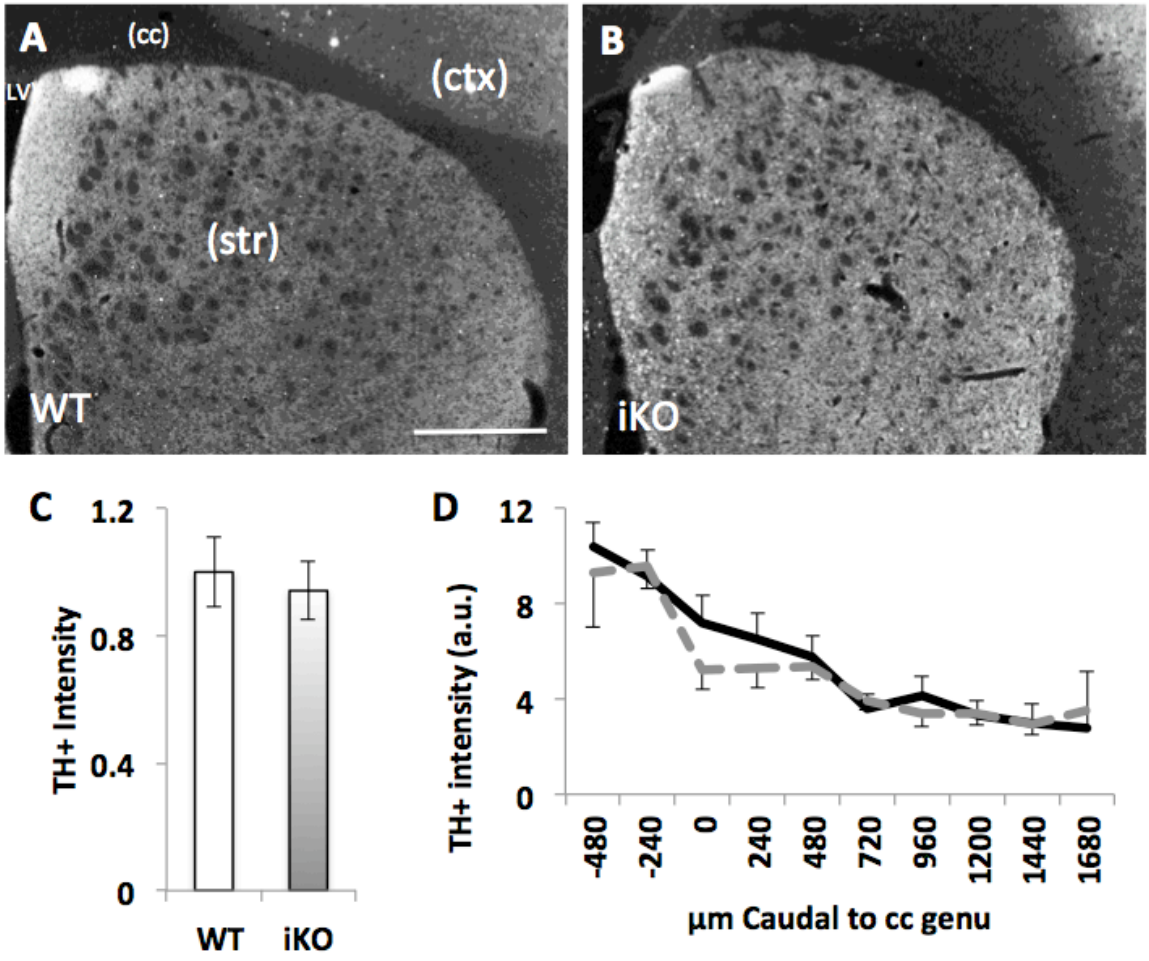

Figure 6. TH+ staining intensity of dopaminergic innervation in the striatum was not different at 5 months after knockout induction.

(A, B) Representative images of TH+ immunostaining in striatum of wild type (A) and induced *ndufs4* knockout (B) animals 5 months after knockout induction. Scale bar: 250 µm for A, B. (C) Quantification of TH immunofluorescence intensity in wild type (open bar) and induced knockout (filled bar) striatum. (D) Quantification of the pattern of TH immunofluorescence of wild type (solid line) and induced knockout mice (dashed line) along the rostrocaudal axis of the striatum. Striatal sections were normalized to the genu of the corpus callosum. Abbreviations: str, striatum; cc, corpus callosum; lv, lateral ventricle; ctx, cortex; a.u., arbitrary units.

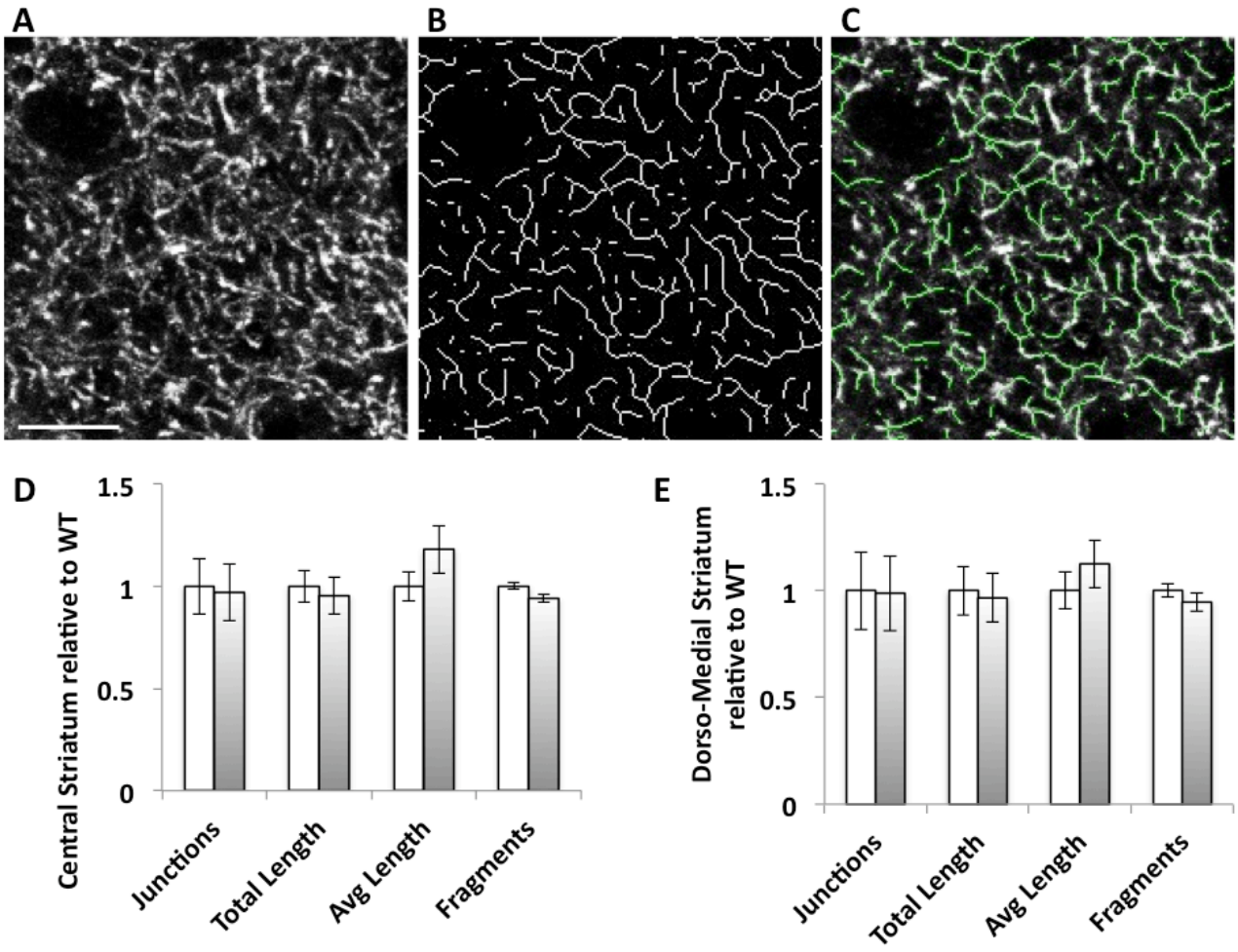

Figure 7. Structure of TH+ axons was not affected at 3 months after *ndufs4* knockout induction.

(A) Representative of confocal image of TH+ axon fibers in the striatum (white). Scale bar: 10 μm for A-C. (B) Skeletonized graph of image in A. (C) Overlay of A (grayscale) and B (green). (D, E) The number of junctions, total length, average length, and count of axon fragments was analyzed by skeletonized model at 3 months after knockout induction. Images were collected from the center (D) or the dorsomedial boundary adjacent to the lateral ventricle and corpus callosum (E) of the striatum at six normalized locations along the rostrocaudal axis. No differences were detected between genotypes using one-way ANOVA.

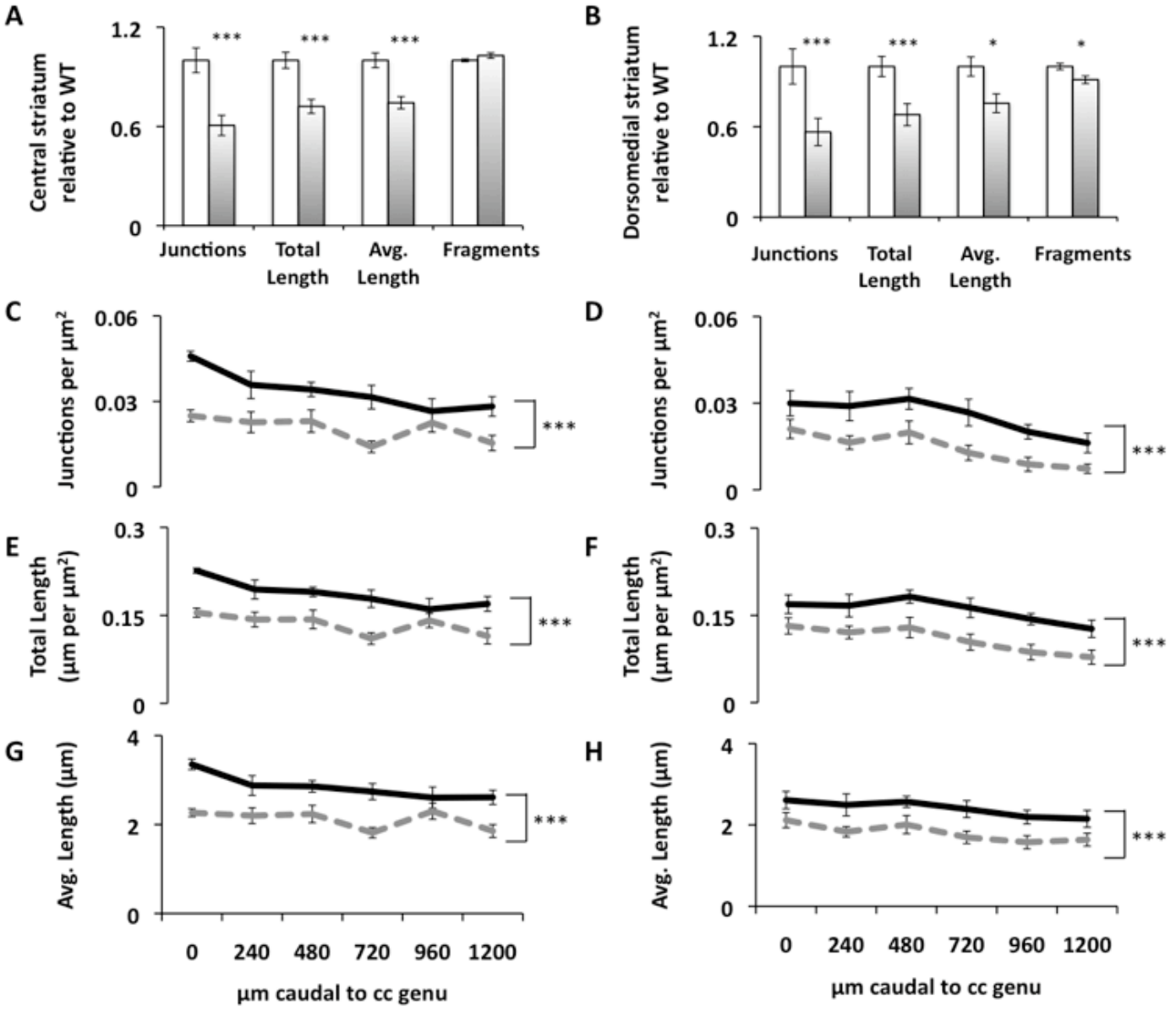

Figure 8. The structural complexity of TH+ axons was reduced in *ndufs4* knockout animals 5 months after knockout induction.

(A) Confocal images of TH+ axons were analyzed by skeletonized model as in Fig. 7. The number of axon junctions, total axon length, and average fragment length was significantly decreased in knockout animals (filled bars) compared with wild type littermates (open bars). Images were collected from the center of coronal sections of the striatum at 6 normalized locations along the rostrocaudal axis. The results are shown pooled from individual animals. (B) A second series of images, collected from the dorsomedial boundary of the striatum was analyzed identically to A. At 5 months after knockout induction at this coronal location, axon structure of knockout animals (filled bars) compared to wild type (open bars) demonstrated significant decreases in number of junctions, total length, average length, and the count of axon fragments. (C, E, G) Axon

structural changes at the central location in the striatum persisted from rostral to caudal within the striatum. The number of junctions (C), total length (E), and average length (G) of fragments was decreased in knockout animals (dashed lines) compared with wild type littermates (solid lines). Sequential sections from each animal were normalized to the genu of the corpus callosum (cc). (D, F, H) Axon structural changes at the dorsomedial location in the striatum also persisted from rostral to caudal within the striatum.

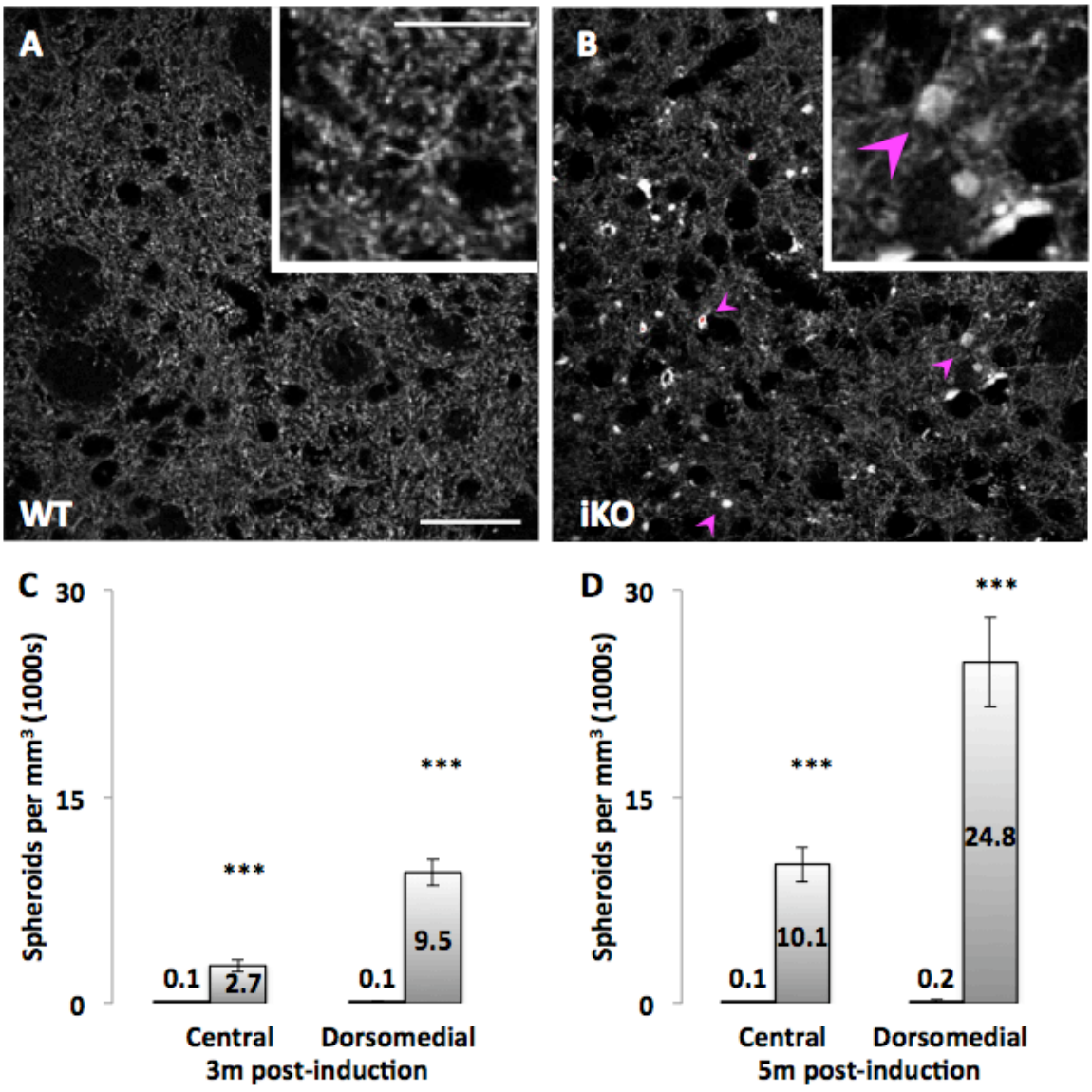

Figure 9. Axonal spheroids formed in the dopamine axons of *ndufs4* knockout.

(A, B) Representative images of wild type (A) and induced knockout (B) dopamine axons in striatum. Spheroids are identified by magenta arrowheads. Scale bar: 40 μm for A, B. Insets: enlarged view. Scale bar: 20 μm. (C) Quantification of the frequency of axonal spheroids in the central or dorsomedial striatum, of wild type (open bars) or knockout (filled bars) animals.

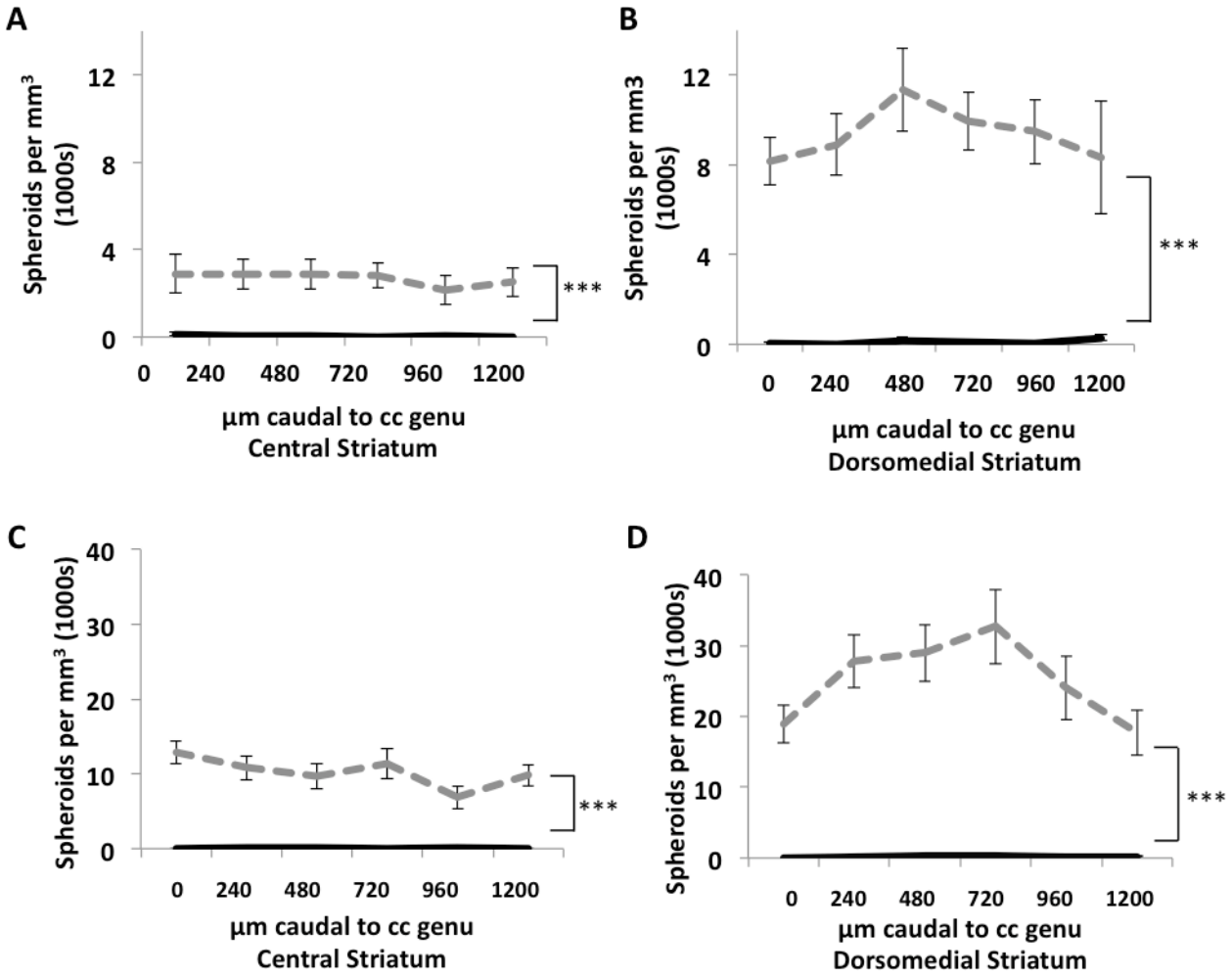

Figure 10. Axonal spheroid formation along the rostrocaudal axis of the striatum.

(A, B) Quantification of axonal spheroids at 3 months after knockout induction in *ndufs4* knockout (dashed lines) or wild type (solid lines) littermates. Images were collected from the center (A) or the dorsomedial boundary (B) of serial coronal sections of the striatum. (C, D) Quantification as in A and B, at 5 months after knockout induction.

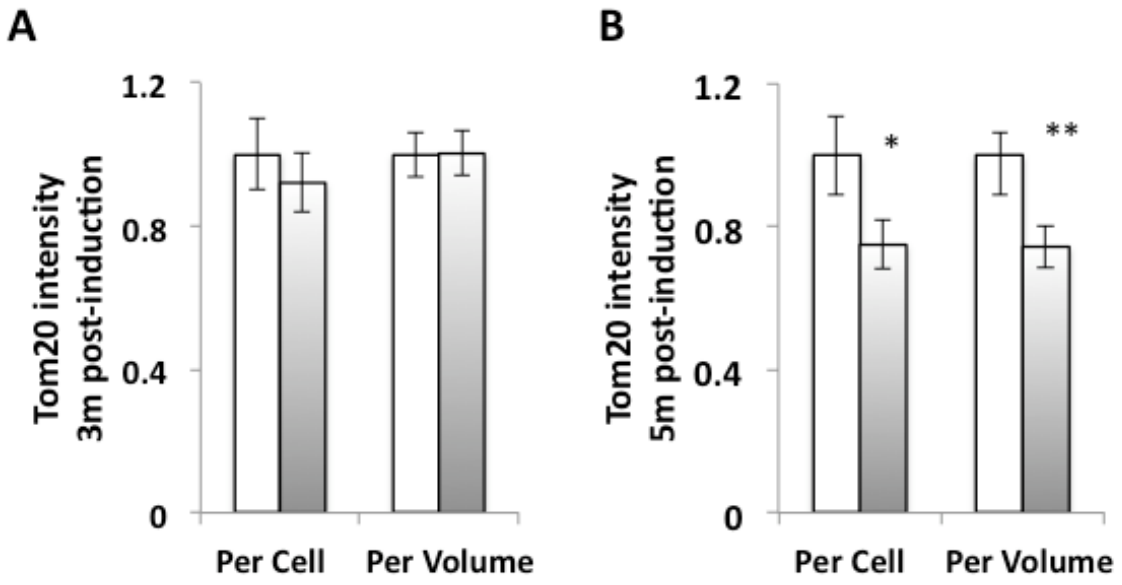

Figure 11. Tom20 immunofluorescence intensity was reduced in *ndufs4* knockout.

(A) Quantification of the intensity of Tom20 staining of single TH+ cells in the SN of wild type (open bars) or knockout (filled bars) animals 3 months after induction of *ndufs4* knockout. (B) Quantification as in A, of wild type (open bars) or knockout (filled bars) littermates 5 months after induction of *ndufs4* knockout. Intensity of fluorescence was not reduced at 3 months after knockout induction, but was reduced at 5 months post-induction.

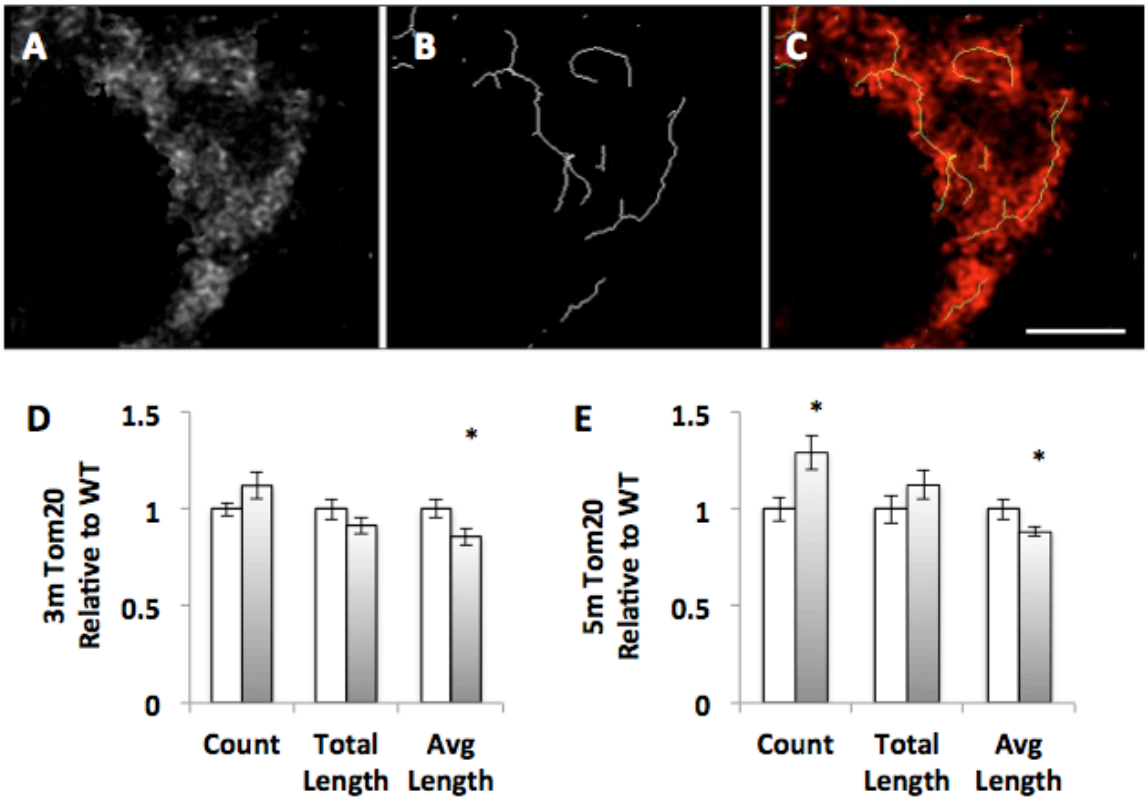

Figure 12. Average length of mitochondrial particles was reduced in TH+ cells of *ndufs4* knockout animals.

(A-C) Representative image of Tom20 staining analyzed by skeletonization model. Tom20 immunofluorescence (A) was converted to 3 dimensional skeletonized graph (B). Overlay (C) with both Tom20 (red) and skeletonized graph (green). Scale bar: 3 μm for A-C. (D, E) The skeletonized structures of mitochondrial particles were measured from TH+ cell bodies in the SN at 3 months (D) and 5 months (E) after *ndufs4* knockout induction. The average length of skeletonized mitochondrial particles was significantly shorter in the TH+ cells of knockout animals (filled bars) compared with wild type littermates (open bars).

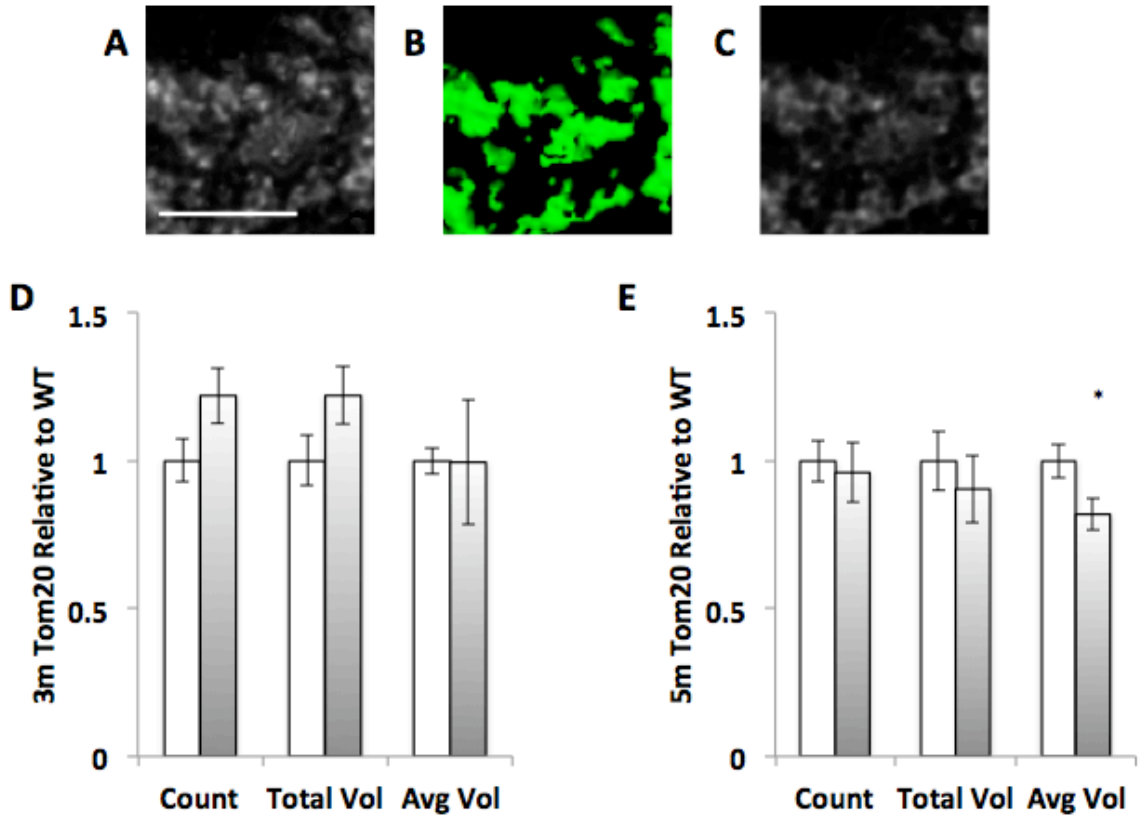

Figure 13. Average volume of mitochondrial particles was reduced at 5 months after knockout induction.

(A-C) Representative images of Tom20 immunostaining analyzed by the space-filling model. A 3 dimensional image stack of Tom20 immunoflourescence is presented using a maximum-intensity projection (A), a 3-dimensional rendering (B), or a single-plane image (C). Scale bar: 3 μm for A-C. (D) No significant difference was observed in count, total volume or average volume of mitochondrial particles labeled by Tom20 immunoreactivity at 3 months after knockout induction between wild type (open bars) and knockout animals (filled bars). (E) At 5 months after knockout induction, a significant decrease in average volume of mitochondrial particles was observed in the TH+ cells of knockout animals (filled bars) compared to wild type littermates (open bars).

APPENDIX

```
dir1 = "/path/to/files/"; // this folder contains a folder for each animal, which
contains a number of oif files and their accompanying folders from Fluoview
outDir = "/path/to/output/"; // this folder will be filled with the data files generated
list = getFileList(dir1);
run("Bio-Formats Macro Extensions");
setBatchMode(true);
for (i=0; i<list.length; i++) [
        dir2 = dir1+list[i];
        list2 = getFileList(dir2);
        for (j=0; j<list2.length; j+=2) [
                fname = list[i]+list2[j];
                Ext.openImagePlus(dir2+list2[j]);
                rename(fname);
                run("Split Channels");
                selectWindow(fname);
                run("Z Project...", "start=1 stop=3 projection=[Max Intensity]");
                selectWindow("MAX_"+fname);
                run("Tubeness", "sigma=0.414 use");
                run("8-bit");
                setThreshold(15, 255);
                run("Convert to Mask");
                run("Skeletonize (2D/3D)");
                saveAs("Jpeg", outDir+fname+".jpg");
                run("Analyze Skeleton (2D/3D)", "prune=none calculate");
                selectWindow("Longest shortest paths");
                saveAs("Results", outDir+fname+".xls");
                close();
                close();
                close();
                close();
        ]
]
```

Figure A1. The ImageJ/Fiji macro used to collect data for the skeletonization assay. The macro takes a folder of confocal stack images and produces a folder of xls spread-sheets containing the analysis of all the skeleton graphs produced, as well as a jpg file showing the resulting skeleton that was used to generate the analysis. The xls spreadsheets are internally tab-delineated text files. The macro should be saved with filename extension "ijm."

```
dir1 = "/path/to/files/";
dir2 = "/path/to/output/";
list = getFileList(dir1);
run("Bio-Formats Macro Extensions");
setBatchMode(true);
for (i=0; i<list.length; i++) [
	fname = list[i];
	aname = substring(fname, 0, lengthOf(fname)-4);
	Ext.openImagePlus(dir1+fname);
	run("Split Channels");
	selectWindow("C2-"+fname);
	rename("TH"+aname);
	resetMinAndMax();
	run("8-bit");
	setThreshold(9, 255);
	run("Convert to Mask", "calculate black");
	run("Divide...", "value=255 stack");
	selectWindow("C1-"+fname);
	rename("TOM"+aname);
	resetMinAndMax();
	run("8-bit");
	imageCalculator("Multiply stack", "TOM"+aname, "TH"+aname);

	run("8-bit");
	run("3D Objects Counter", "threshold=30 slice=1 min.=10 max.=Infinity
exclude_objects_on_edges objects statistics summary");
	selectWindow("Statistics for TOM"+aname);
	saveAs("Results", dir2+aname+"TOM.xls");
	selectWindow("Objects map of TOM"+aname);
	run("8-bit");
	setMinAndMax(0, 22);
	call("ij.ImagePlus.setDefault16bitRange", 0);
	run("Z Project...", "start=1 projection=[Max Intensity]");
	selectWindow("MAX_Objects map of tubeness of TOM"+aname);
	saveAs("PNG", dir2+aname+"TOMMAP.png");
	close();

	selectWindow("TOM"+aname);
	run("Tubeness", "sigma=0.3 use"); // sigma is the expected width of tubes
	selectWindow("tubeness of TOM"+aname);
	setAutoThreshold("Default dark");
	setThreshold(15, 255);
	run("Convert to Mask", "  black");
	run("Skeletonize (2D/3D)");
	run("Z Project...", "start=1 projection=[Max Intensity]");
	selectWindow("MAX_tubeness of TOM"+aname);
	saveAs("Jpeg", dir2+aname+"skel.jpg");
	run("Analyze Skeleton (2D/3D)", "prune=none calculate");
	selectWindow("Longest shortest paths");
	saveAs("Results", dir2+aname+"skel.xls");
	close(); close(); close(); close(); close(); close();
]
beep();
```

Figure A2. The ImageJ/Fiji macro used to collect data for the mitochondria assay. The macro takes a folder of deconvolved confocal stack images and produces a folder of xls spread-sheets containing the analysis of all the 3D object analyses produced, as well as a jpg file showing the resulting object map that was used to generate the numbers. The xls spreadsheets are internally tab-delineated text files. The macro should be saved with filename extension “ijm.”

REFERENCES

Adle-Biassette H, Chretien F, Wingertsmann L, Hery C, Ereau T, Scaravilli F, Tardieu M, Gray F. 1999. Neuronal apoptosis does not correlate with dementia in HIV infection but is related to microglial activation and axonal damage. Neuropathol Appl Neurobiol 25(2):123-133.

Alam M, Schmidt WJ. 2002. Rotenone destroys dopaminergic neurons and induces parkinsonian symptoms in rats. Behav Brain Res 136(1):317-324.

Alberio T, Lopiano L, Fasano M. 2012. Cellular models to investigate biochemical pathways in Parkinson's disease. FEBS J 279(7):1146-1155.

Arganda-Carreras I, Fernandez-Gonzalez R, Munoz-Barrutia A, Ortiz-De-Solorzano C. 2010. 3D reconstruction of histological sections: Application to mammary gland tissue. Microsc Res Tech 73(11):1019-1029.

Assouline Z, Jambou M, Rio M, Bole-Feysot C, de Lonlay P, Barnerias C, Desguerre I, Bonnemains C, Guillermet C, Steffann J, Munnich A, Bonnefont JP, Rotig A, Lebre AS. 2012. A constant and similar assembly defect of mitochondrial respiratory chain complex I allows rapid identification of NDUFS4 mutations in patients with Leigh syndrome. Biochim Biophys Acta 1822(6):1062-1069.

Baquet ZC, Williams D, Brody J, Smeyne RJ. 2009. A comparison of model-based (2D) and design-based (3D) stereological methods for estimating cell number in the substantia nigra pars compacta (SNpc) of the C57BL/6J mouse. Neuroscience 161(4):1082-1090.

Barber-Singh J, Seo BB, Nakamaru-Ogiso E, Lau YS, Matsuno-Yagi A, Yagi T. 2009. Neuroprotective effect of long-term NDI1 gene expression in a chronic mouse model of Parkinson disorder. Rejuvenation Res 12(4):259-267.

Barnum CJ, Tansey MG. 2010. Modeling neuroinflammatory pathogenesis of Parkinson's disease. Prog Brain Res 184:113-132.

Barsoum MJ, Yuan H, Gerencser AA, Liot G, Kushnareva Y, Graber S, Kovacs I, Lee WD, Waggoner J, Cui J, White AD, Bossy B, Martinou JC, Youle RJ, Lipton SA, Ellisman MH, Perkins GA, Bossy-Wetzel E. 2006. Nitric oxide-induced mitochondrial fission is regulated by dynamin-related GTPases in neurons. EMBO J 25(16):3900-3911.

Benard G, Bellance N, James D, Parrone P, Fernandez H, Letellier T, Rossignol R. 2007. Mitochondrial bioenergetics and structural network organization. J Cell Sci 120(Pt 5):838-848.

Betarbet R, Sherer TB, MacKenzie G, Garcia-Osuna M, Panov AV, Greenamyre JT. 2000. Chronic systemic pesticide exposure reproduces features of Parkinson's disease. Nat Neurosci 3(12):1301-1306.

Blackstone C, Chang CR. 2011. Mitochondria unite to survive. Nat Cell Biol 13(5):521-522.

Braak H, Del Tredici K, Rub U, de Vos RA, Jansen Steur EN, Braak E. 2003. Staging of brain pathology related to sporadic Parkinson's disease. Neurobiol Aging 24(2):197-211.

Budde SM, van den Heuvel LP, Janssen AJ, Smeets RJ, Buskens CA, DeMeirleir L, Van Coster R, Baethmann M, Voit T, Trijbels JM, Smeitink JA. 2000. Combined

enzymatic complex I and III deficiency associated with mutations in the nuclear encoded NDUFS4 gene. Biochem Biophys Res Commun 275(1):63-68.
Carvey PM, Punati A, Newman MB. 2006. Progressive dopamine neuron loss in Parkinson's disease: the multiple hit hypothesis. Cell Transplant 15(3):239-250.
Castillo-Quan JI. 2011. Parkin' control: regulation of PGC-1alpha through PARIS in Parkinson's disease. Dis Model Mech 4(4):427-429.
Caudle WM, Zhang J. 2009. Glutamate, excitotoxicity, and programmed cell death in Parkinson disease. Exp Neurol 220(2):230-233.
Celotto AM, Chiu WK, Van Voorhies W, Palladino MJ. 2011. Modes of metabolic compensation during mitochondrial disease using the Drosophila model of ATP6 dysfunction. PLoS One 6(10):e25823.
Chandra D, Bratton SB, Person MD, Tian Y, Martin AG, Ayres M, Fearnhead HO, Gandhi V, Tang DG. 2006. Intracellular nucleotides act as critical prosurvival factors by binding to cytochrome C and inhibiting apoptosome. Cell 125(7):1333-1346.
Cheng CL, Povlishock JT. 1988. The effect of traumatic brain injury on the visual system: a morphologic characterization of reactive axonal change. J Neurotrauma 5(1):47-60.
Cheng HC, Kim SR, Oo TF, Kareva T, Yarygina O, Rzhetskaya M, Wang C, During M, Talloczy Z, Tanaka K, Komatsu M, Kobayashi K, Okano H, Kholodilov N, Burke RE. 2011. Akt suppresses retrograde degeneration of dopaminergic axons by inhibition of macroautophagy. J Neurosci 31(6):2125-2135.
Cheng HC, Ulane CM, Burke RE. 2010. Clinical progression in Parkinson disease and the neurobiology of axons. Ann Neurol 67(6):715-725.
Choi WS, Kruse SE, Palmiter RD, Xia Z. 2008. Mitochondrial complex I inhibition is not required for dopaminergic neuron death induced by rotenone, MPP+, or paraquat. Proc Natl Acad Sci U S A 105(39):15136-15141.
Choi WS, Palmiter RD, Xia Z. 2011. Loss of mitochondrial complex I activity potentiates dopamine neuron death induced by microtubule dysfunction in a Parkinson's disease model. J Cell Biol 192(5):873-882.
Cicchetti F, Drouin-Ouellet J, Gross RE. 2009. Environmental toxins and Parkinson's disease: what have we learned from pesticide-induced animal models? Trends Pharmacol Sci 30(9):475-483.
Cleeter MW, Cooper JM, Schapira AH. 1992. Irreversible inhibition of mitochondrial complex I by 1-methyl-4-phenylpyridinium: evidence for free radical involvement. J Neurochem 58(2):786-789.
Cole NB, Dieuliis D, Leo P, Mitchell DC, Nussbaum RL. 2008. Mitochondrial translocation of alpha-synuclein is promoted by intracellular acidification. Exp Cell Res 314(10):2076-2089.
Coleman M. 2005. Axon degeneration mechanisms: commonality amid diversity. Nat Rev Neurosci 6(11):889-898.
Cookson MR. 2010. DJ-1, PINK1, and their effects on mitochondrial pathways. Mov Disord 25 Suppl 1:S44-48.
Dauer W, Przedborski S. 2003. Parkinson's disease: mechanisms and models. Neuron 39(6):889-909.

Derijard B, Hibi M, Wu IH, Barrett T, Su B, Deng T, Karin M, Davis RJ. 1994. JNK1: a protein kinase stimulated by UV light and Ha-Ras that binds and phosphorylates the c-Jun activation domain. Cell 76(6):1025-1037.

Devi L, Raghavendran V, Prabhu BM, Avadhani NG, Anandatheerthavarada HK. 2008. Mitochondrial import and accumulation of alpha-synuclein impair complex I in human dopaminergic neuronal cultures and Parkinson disease brain. J Biol Chem 283(14):9089-9100.

Fearnley JM, Lees AJ. 1991. Ageing and Parkinson's disease: substantia nigra regional selectivity. Brain 114 (Pt 5):2283-2301.

Ferguson B, Matyszak MK, Esiri MM, Perry VH. 1997. Axonal damage in acute multiple sclerosis lesions. Brain 120 (Pt 3):393-399.

Fornai F, Schluter OM, Lenzi P, Gesi M, Ruffoli R, Ferrucci M, Lazzeri G, Busceti CL, Pontarelli F, Battaglia G, Pellegrini A, Nicoletti F, Ruggieri S, Paparelli A, Sudhof TC. 2005. Parkinson-like syndrome induced by continuous MPTP infusion: convergent roles of the ubiquitin-proteasome system and alpha-synuclein. Proc Natl Acad Sci U S A 102(9):3413-3418.

Galvin JE, Uryu K, Lee VM, Trojanowski JQ. 1999. Axon pathology in Parkinson's disease and Lewy body dementia hippocampus contains alpha-, beta-, and gamma-synuclein. Proc Natl Acad Sci U S A 96(23):13450-13455.

Gegg ME, Cooper JM, Schapira AH, Taanman JW. 2009. Silencing of PINK1 expression affects mitochondrial DNA and oxidative phosphorylation in dopaminergic cells. PLoS One 4(3):e4756.

Gomes LC, Di Benedetto G, Scorrano L. 2011. During autophagy mitochondria elongate, are spared from degradation and sustain cell viability. Nat Cell Biol 13(5):589-598.

Gradinaru V, Mogri M, Thompson KR, Henderson JM, Deisseroth K. 2009. Optical deconstruction of parkinsonian neural circuitry. Science 324(5925):354-359.

Greenamyre JT, Cannon JR, Drolet R, Mastroberardino PG. 2010. Lessons from the rotenone model of Parkinson's disease. Trends Pharmacol Sci 31(4):141-142; author reply 142-143.

Greffard S, Verny M, Bonnet AM, Beinis JY, Gallinari C, Meaume S, Piette F, Hauw JJ, Duyckaerts C. 2006. Motor score of the Unified Parkinson Disease Rating Scale as a good predictor of Lewy body-associated neuronal loss in the substantia nigra. Arch Neurol 63(4):584-588.

Grohm J, Kim SW, Mamrak U, Tobaben S, Cassidy-Stone A, Nunnari J, Plesnila N, Culmsee C. 2012. Inhibition of Drp1 provides neuroprotection in vitro and in vivo. Cell Death Differ.

Grunewald A, Arns B, Seibler P, Rakovic A, Munchau A, Ramirez A, Sue CM, Klein C. 2012. ATP13A2 mutations impair mitochondrial function in fibroblasts from patients with Kufor-Rakeb syndrome. Neurobiol Aging 33(8):1843 e1841-1847.

Hastings TG, Lewis DA, Zigmond MJ. 1996. Role of oxidation in the neurotoxic effects of intrastriatal dopamine injections. Proc Natl Acad Sci U S A 93(5):1956-1961.

Hayashi T, Ishimori C, Takahashi-Niki K, Taira T, Kim YC, Maita H, Maita C, Ariga H, Iguchi-Ariga SM. 2009. DJ-1 binds to mitochondrial complex I and maintains its activity. Biochem Biophys Res Commun 390(3):667-672.

Henchcliffe C, Beal MF. 2008. Mitochondrial biology and oxidative stress in Parkinson disease pathogenesis. Nat Clin Pract Neurol 4(11):600-609.

Heo JY, Park JH, Kim SJ, Seo KS, Han JS, Lee SH, Kim JM, Park JI, Park SK, Lim K, Hwang BD, Shong M, Kweon GR. 2012. DJ-1 null dopaminergic neuronal cells exhibit defects in mitochondrial function and structure: involvement of mitochondrial complex I assembly. PLoS One 7(3):e32629.

Hernandez JP, Xu F, Frazier DT. 2004. Medial vestibular nucleus mediates the cardiorespiratory responses to fastigial nuclear activation and hypercapnia. J Appl Physiol 97(3):835-842.

Hoglinger GU, Oertel WH, Hirsch EC. 2006. The rotenone model of parkinsonism--the five years inspection. J Neural Transm Suppl(70):269-272.

Hurley MJ, Dexter DT. 2012. Voltage-gated calcium channels and Parkinson's disease. Pharmacol Ther 133(3):324-333.

Inden M, Kitamura Y, Abe M, Tamaki A, Takata K, Taniguchi T. 2011. Parkinsonian rotenone mouse model: reevaluation of long-term administration of rotenone in C57BL/6 mice. Biol Pharm Bull 34(1):92-96.

Inden M, Kitamura Y, Takeuchi H, Yanagida T, Takata K, Kobayashi Y, Taniguchi T, Yoshimoto K, Kaneko M, Okuma Y, Taira T, Ariga H, Shimohama S. 2007. Neurodegeneration of mouse nigrostriatal dopaminergic system induced by repeated oral administration of rotenone is prevented by 4-phenylbutyrate, a chemical chaperone. J Neurochem 101(6):1491-1504.

Ishihara N, Nomura M, Jofuku A, Kato H, Suzuki SO, Masuda K, Otera H, Nakanishi Y, Nonaka I, Goto Y, Taguchi N, Morinaga H, Maeda M, Takayanagi R, Yokota S, Mihara K. 2009. Mitochondrial fission factor Drp1 is essential for embryonic development and synapse formation in mice. Nat Cell Biol 11(8):958-966.

Jain S, Goldstein DS. 2012. What ARE Parkinson disease? Non-motor features transform conception of the shaking palsy. Neurobiol Dis 46(3):505-507.

Javitch JA, D'Amato RJ, Strittmatter SM, Snyder SH. 1985. Parkinsonism-inducing neurotoxin, N-methyl-4-phenyl-1,2,3,6 -tetrahydropyridine: uptake of the metabolite N-methyl-4-phenylpyridine by dopamine neurons explains selective toxicity. Proc Natl Acad Sci U S A 82(7):2173-2177.

Jenner P. 2003. Oxidative stress in Parkinson's disease. Ann Neurol 53 Suppl 3:S26-36; discussion S36-28.

Kageyama Y, Zhang Z, Roda R, Fukaya M, Wakabayashi J, Wakabayashi N, Kensler TW, Reddy PH, Iijima M, Sesaki H. 2012. Mitochondrial division ensures the survival of postmitotic neurons by suppressing oxidative damage. J Cell Biol 197(4):535-551.

Keeney PM, Xie J, Capaldi RA, Bennett JP, Jr. 2006. Parkinson's disease brain mitochondrial complex I has oxidatively damaged subunits and is functionally impaired and misassembled. J Neurosci 26(19):5256-5264.

Koopman WJ, Visch HJ, Verkaart S, van den Heuvel LW, Smeitink JA, Willems PH. 2005. Mitochondrial network complexity and pathological decrease in complex I activity are tightly correlated in isolated human complex I deficiency. Am J Physiol Cell Physiol 289(4):C881-890.

Kruse SE, Watt WC, Marcinek DJ, Kapur RP, Schenkman KA, Palmiter RD. 2008. Mice with mitochondrial complex I deficiency develop a fatal encephalomyopathy. Cell Metab 7(4):312-320.

Kuhn W, Muller T, Winkel R, Danielczik S, Gerstner A, Hacker R, Mattern C, Przuntek H. 1996. Parenteral application of NADH in Parkinson's disease: clinical improvement partially due to stimulation of endogenous levodopa biosynthesis. J Neural Transm 103(10):1187-1193.

Langston JW, Ballard P, Tetrud JW, Irwin I. 1983. Chronic Parkinsonism in humans due to a product of meperidine-analog synthesis. Science 219(4587):979-980.

Langston JW, Ballard PA, Jr. 1983. Parkinson's disease in a chemist working with 1-methyl-4-phenyl-1,2,5,6-tetrahydropyridine. N Engl J Med 309(5):310.

Lee CS, Samii A, Sossi V, Ruth TJ, Schulzer M, Holden JE, Wudel J, Pal PK, de la Fuente-Fernandez R, Calne DB, Stoessl AJ. 2000. In vivo positron emission tomographic evidence for compensatory changes in presynaptic dopaminergic nerve terminals in Parkinson's disease. Ann Neurol 47(4):493-503.

Lesage S, Brice A. 2009. Parkinson's disease: from monogenic forms to genetic susceptibility factors. Hum Mol Genet 18(R1):R48-59.

Li H, Li SH, Yu ZX, Shelbourne P, Li XJ. 2001. Huntingtin aggregate-associated axonal degeneration is an early pathological event in Huntington's disease mice. J Neurosci 21(21):8473-8481.

Li LH, Qin HZ, Wang JL, Wang J, Wang XL, Gao GD. 2009a. Axonal degeneration of nigra-striatum dopaminergic neurons induced by 1-methyl-4-phenyl-1,2,3,6-tetrahydropyridine in mice. J Int Med Res 37(2):455-463.

Li N, Ragheb K, Lawler G, Sturgis J, Rajwa B, Melendez JA, Robinson JP. 2003. Mitochondrial complex I inhibitor rotenone induces apoptosis through enhancing mitochondrial reactive oxygen species production. J Biol Chem 278(10):8516-8525.

Li Y, Liu W, Oo TF, Wang L, Tang Y, Jackson-Lewis V, Zhou C, Geghman K, Bogdanov M, Przedborski S, Beal MF, Burke RE, Li C. 2009b. Mutant LRRK2(R1441G) BAC transgenic mice recapitulate cardinal features of Parkinson's disease. Nat Neurosci 12(7):826-828.

Liberski PP, Budka H. 1999. Neuroaxonal pathology in Creutzfeldt-Jakob disease. Acta Neuropathol 97(4):329-334.

Loeb V, Yakunin E, Saada A, Sharon R. 2010. The transgenic overexpression of alpha-synuclein and not its related pathology associates with complex I inhibition. J Biol Chem 285(10):7334-7343.

Lutz AK, Exner N, Fett ME, Schlehe JS, Kloos K, Lammermann K, Brunner B, Kurz-Drexler A, Vogel F, Reichert AS, Bouman L, Vogt-Weisenhorn D, Wurst W, Tatzelt J, Haass C, Winklhofer KF. 2009. Loss of parkin or PINK1 function increases Drp1-dependent mitochondrial fragmentation. J Biol Chem 284(34):22938-22951.

M. Angela Cenci ML. 2005. Animal Models of Movement Disorders. In: LeDoux M, editor. Animal Models of Movement Disorders: Elsevier Academic Press. p 1.

Macaya A, Munell F, Burke RE, De Vivo DC. 1993. Disorders of movement in Leigh syndrome. Neuropediatrics 24(2):60-67.

MacLeod D, Dowman J, Hammond R, Leete T, Inoue K, Abeliovich A. 2006. The familial Parkinsonism gene LRRK2 regulates neurite process morphology. Neuron 52(4):587-593.

Marella M, Seo BB, Nakamaru-Ogiso E, Greenamyre JT, Matsuno-Yagi A, Yagi T. 2008. Protection by the NDI1 gene against neurodegeneration in a rotenone rat model of Parkinson's disease. PLoS One 3(1):e1433.

Marshall LE, Himes RH. 1978. Rotenone inhibition of tubulin self-assembly. Biochim Biophys Acta 543(4):590-594.

Martin LJ, Pan Y, Price AC, Sterling W, Copeland NG, Jenkins NA, Price DL, Lee MK. 2006. Parkinson's disease alpha-synuclein transgenic mice develop neuronal mitochondrial degeneration and cell death. J Neurosci 26(1):41-50.

Matsuda W, Furuta T, Nakamura KC, Hioki H, Fujiyama F, Arai R, Kaneko T. 2009. Single nigrostriatal dopaminergic neurons form widely spread and highly dense axonal arborizations in the neostriatum. J Neurosci 29(2):444-453.

Meredith GE, Kang UJ. 2006. Behavioral models of Parkinson's disease in rodents: a new look at an old problem. Mov Disord 21(10):1595-1606.

Miyazaki I, Asanuma M. 2008. Dopaminergic neuron-specific oxidative stress caused by dopamine itself. Acta Med Okayama 62(3):141-150.

Mizuno Y, Ohta S, Tanaka M, Takamiya S, Suzuki K, Sato T, Oya H, Ozawa T, Kagawa Y. 1989. Deficiencies in complex I subunits of the respiratory chain in Parkinson's disease. Biochem Biophys Res Commun 163(3):1450-1455.

Morais VA, Verstreken P, Roethig A, Smet J, Snellinx A, Vanbrabant M, Haddad D, Frezza C, Mandemakers W, Vogt-Weisenhorn D, Van Coster R, Wurst W, Scorrano L, De Strooper B. 2009. Parkinson's disease mutations in PINK1 result in decreased Complex I activity and deficient synaptic function. EMBO Mol Med 1(2):99-111.

Moretto A, Colosio C. 2011. Biochemical and toxicological evidence of neurological effects of pesticides: the example of Parkinson's disease. Neurotoxicology 32(4):383-391.

Mortiboys H, Johansen KK, Aasly JO, Bandmann O. 2010. Mitochondrial impairment in patients with Parkinson disease with the G2019S mutation in LRRK2. Neurology 75(22):2017-2020.

Nakada K, Inoue K, Ono T, Isobe K, Ogura A, Goto YI, Nonaka I, Hayashi JI. 2001. Inter-mitochondrial complementation: Mitochondria-specific system preventing mice from expression of disease phenotypes by mutant mtDNA. Nat Med 7(8):934-940.

Nakamura K, Nemani VM, Azarbal F, Skibinski G, Levy JM, Egami K, Munishkina L, Zhang J, Gardner B, Wakabayashi J, Sesaki H, Cheng Y, Finkbeiner S, Nussbaum RL, Masliah E, Edwards RH. 2011. Direct membrane association drives mitochondrial fission by the Parkinson disease-associated protein alpha-synuclein. J Biol Chem 286(23):20710-20726.

Nicklas WJ, Youngster SK, Kindt MV, Heikkila RE. 1987. MPTP, MPP+ and mitochondrial function. Life Sci 40(8):721-729.

Nishioka K, Vilarino-Guell C, Cobb SA, Kachergus JM, Ross OA, Hentati E, Hentati F, Farrer MJ. 2010. Genetic variation of the mitochondrial complex I subunit NDUFV2 and Parkinson's disease. Parkinsonism Relat Disord 16(10):686-687.

Olanow CW, McNaught K. 2011. Parkinson's disease, proteins, and prions: milestones. Mov Disord 26(6):1056-1071.

Ozaki N, Nakahara D, Mogi M, Harada M, Kiuchi K, Kaneda N, Miura Y, Kasahara Y, Nagatsu T. 1988. Inactivation of tyrosine hydroxylase in rat striatum by 1-methyl-4-phenylpyridinium ion (MPP+). Neurosci Lett 85(2):228-232.

Pallanck LJ. 2010. Culling sick mitochondria from the herd. J Cell Biol 191(7):1225-1227.

Parisiadou L, Xie C, Cho HJ, Lin X, Gu XL, Long CX, Lobbestael E, Baekelandt V, Taymans JM, Sun L, Cai H. 2009. Phosphorylation of ezrin/radixin/moesin proteins by LRRK2 promotes the rearrangement of actin cytoskeleton in neuronal morphogenesis. J Neurosci 29(44):13971-13980.

Parker WD, Jr., Boyson SJ, Parks JK. 1989. Abnormalities of the electron transport chain in idiopathic Parkinson's disease. Ann Neurol 26(6):719-723.

Perales-Clemente E, Bayona-Bafaluy MP, Perez-Martos A, Barrientos A, Fernandez-Silva P, Enriquez JA. 2008. Restoration of electron transport without proton pumping in mammalian mitochondria. Proc Natl Acad Sci U S A 105(48):18735-18739.

Pifl C, Giros B, Caron MG. 1993. Dopamine transporter expression confers cytotoxicity to low doses of the parkinsonism-inducing neurotoxin 1-methyl-4-phenylpyridinium. J Neurosci 13(10):4246-4253.

Piggott MA, Marshall EF, Thomas N, Lloyd S, Court JA, Jaros E, Burn D, Johnson M, Perry RH, McKeith IG, Ballard C, Perry EK. 1999a. Striatal dopaminergic markers in dementia with Lewy bodies, Alzheimer's and Parkinson's diseases: rostrocaudal distribution. Brain 122 (Pt 8):1449-1468.

Piggott MA, Marshall EF, Thomas N, Lloyd S, Court JA, Jaros E, Costa D, Perry RH, Perry EK. 1999b. Dopaminergic activities in the human striatum: rostrocaudal gradients of uptake sites and of D1 and D2 but not of D3 receptor binding or dopamine. Neuroscience 90(2):433-445.

Quintana A, Kruse SE, Kapur RP, Sanz E, Palmiter RD. 2010. Complex I deficiency due to loss of Ndufs4 in the brain results in progressive encephalopathy resembling Leigh syndrome. Proc Natl Acad Sci U S A 107(24):10996-11001.

Quintana A, Zanella S, Koch H, Kruse SE, Lee D, Ramirez JM, Palmiter RD. 2012. Fatal breathing dysfunction in a mouse model of Leigh syndrome. J Clin Invest.

Ramonet D, Daher JP, Lin BM, Stafa K, Kim J, Banerjee R, Westerlund M, Pletnikova O, Glauser L, Yang L, Liu Y, Swing DA, Beal MF, Troncoso JC, McCaffery JM, Jenkins NA, Copeland NG, Galter D, Thomas B, Lee MK, Dawson TM, Dawson VL, Moore DJ. 2012. Dopaminergic neuronal loss, reduced neurite complexity and autophagic abnormalities in transgenic mice expressing G2019S mutant LRRK2. PLoS One 6(4):e18568.

Rea MA, Simon JR. 1981. Regional distribution of cholinergic parameters within the rat striatum. Brain Res 219(2):317-326.

Riederer P, Wuketich S. 1976. Time course of nigrostriatal degeneration in parkinson's disease. A detailed study of influential factors in human brain amine analysis. J Neural Transm 38(3-4):277-301.

Sato Y, Nakajima S, Shiraga N, Atsumi H, Yoshida S, Koller T, Gerig G, Kikinis R. 1998. Three-dimensional multi-scale line filter for segmentation and visualization of curvilinear structures in medical images. Med Image Anal 2(2):143-168.

Saxton WM, Hollenbeck PJ. 2012. The axonal transport of mitochondria. J Cell Sci 125(Pt 9):2095-2104.

Scacco S, Petruzzella V, Budde S, Vergari R, Tamborra R, Panelli D, van den Heuvel LP, Smeitink JA, Papa S. 2003. Pathological mutations of the human NDUFS4 gene of the 18-kDa (AQDQ) subunit of complex I affect the expression of the protein and the assembly and function of the complex. J Biol Chem 278(45):44161-44167.

Schapira AH. 2011. Mitochondrial pathology in Parkinson's disease. Mt Sinai J Med 78(6):872-881.

Scherman D, Desnos C, Darchen F, Pollak P, Javoy-Agid F, Agid Y. 1989. Striatal dopamine deficiency in Parkinson's disease: role of aging. Ann Neurol 26(4):551-557.

Schmidt WJ, Alam M. 2006. Controversies on new animal models of Parkinson's disease pro and con: the rotenone model of Parkinson's disease (PD). J Neural Transm Suppl(70):273-276.

Seo BB, Nakamaru-Ogiso E, Flotte TR, Matsuno-Yagi A, Yagi T. 2006. In vivo complementation of complex I by the yeast Ndi1 enzyme. Possible application for treatment of Parkinson disease. J Biol Chem 281(20):14250-14255.

Sherer TB, Richardson JR, Testa CM, Seo BB, Panov AV, Yagi T, Matsuno-Yagi A, Miller GW, Greenamyre JT. 2007. Mechanism of toxicity of pesticides acting at complex I: relevance to environmental etiologies of Parkinson's disease. J Neurochem 100(6):1469-1479.

Shin JH, Ko HS, Kang H, Lee Y, Lee YI, Pletinkova O, Troconso JC, Dawson VL, Dawson TM. 2011. PARIS (ZNF746) repression of PGC-1alpha contributes to neurodegeneration in Parkinson's disease. Cell 144(5):689-702.

Sidiropoulos C, Walsh R, Meoni S, Moro E. 2012. Surgical treatment of Parkinson's disease. Curr Treat Options Neurol 14(3):211-212.

Spillantini MG, Schmidt ML, Lee VM, Trojanowski JQ, Jakes R, Goedert M. 1997. Alpha-synuclein in Lewy bodies. Nature 388(6645):839-840.

Sterky FH, Hoffman AF, Milenkovic D, Bao B, Paganelli A, Edgar D, Wibom R, Lupica CR, Olson L, Larsson NG. 2011. Altered dopamine metabolism and increased vulnerability to MPTP in mice with partial deficiency of mitochondrial complex I in dopamine neurons. Hum Mol Genet 21(5):1078-1089.

Stoessl AJ, Martin WW, McKeown MJ, Sossi V. 2011. Advances in imaging in Parkinson's disease. Lancet Neurol 10(11):987-1001.

Stokin GB, Lillo C, Falzone TL, Brusch RG, Rockenstein E, Mount SL, Raman R, Davies P, Masliah E, Williams DS, Goldstein LS. 2005. Axonopathy and transport deficits early in the pathogenesis of Alzheimer's disease. Science 307(5713):1282-1288.

Tagliati M, Martin C, Alterman R. 2010. Lack of motor symptoms progression in Parkinson's disease patients with long-term bilateral subthalamic deep brain stimulation. Int J Neurosci 120(11):717-723.

Thomas KJ, McCoy MK, Blackinton J, Beilina A, van der Brug M, Sandebring A, Miller D, Maric D, Cedazo-Minguez A, Cookson MR. 2011. DJ-1 acts in parallel to the PINK1/parkin pathway to control mitochondrial function and autophagy. Hum Mol Genet 20(1):40-50.

Tieu K, Perier C, Caspersen C, Teismann P, Wu DC, Yan SD, Naini A, Vila M, Jackson-Lewis V, Ramasamy R, Przedborski S. 2003. D-beta-hydroxybutyrate rescues

mitochondrial respiration and mitigates features of Parkinson disease. J Clin Invest 112(6):892-901.

Trapp BD, Peterson J, Ransohoff RM, Rudick R, Mork S, Bo L. 1998. Axonal transection in the lesions of multiple sclerosis. N Engl J Med 338(5):278-285.

Tsai J, Grutzendler J, Duff K, Gan WB. 2004. Fibrillar amyloid deposition leads to local synaptic abnormalities and breakage of neuronal branches. Nat Neurosci 7(11):1181-1183.

Twig G, Elorza A, Molina AJ, Mohamed H, Wikstrom JD, Walzer G, Stiles L, Haigh SE, Katz S, Las G, Alroy J, Wu M, Py BF, Yuan J, Deeney JT, Corkey BE, Shirihai OS. 2008. Fission and selective fusion govern mitochondrial segregation and elimination by autophagy. EMBO J 27(2):433-446.

Van Bergen NJ, Crowston JG, Kearns LS, Staffieri SE, Hewitt AW, Cohn AC, Mackey DA, Trounce IA. 2011. Mitochondrial oxidative phosphorylation compensation may preserve vision in patients with OPA1-linked autosomal dominant optic atrophy. PLoS One 6(6):e21347.

van den Heuvel L, Ruitenbeek W, Smeets R, Gelman-Kohan Z, Elpeleg O, Loeffen J, Trijbels F, Mariman E, de Bruijn D, Smeitink J. 1998. Demonstration of a new pathogenic mutation in human complex I deficiency: a 5-bp duplication in the nuclear gene encoding the 18-kD (AQDQ) subunit. Am J Hum Genet 62(2):262-268.

Vrecko K, Storga D, Birkmayer JG, Moller R, Tafeit E, Horejsi R, Reibnegger G. 1997. NADH stimulates endogenous dopamine biosynthesis by enhancing the recycling of tetrahydrobiopterin in rat phaeochromocytoma cells. Biochim Biophys Acta 1361(1):59-65.

Wang X, Petrie TG, Liu Y, Liu J, Fujioka H, Zhu X. 2012. Parkinson's disease-associated DJ-1 mutations impair mitochondrial dynamics and cause mitochondrial dysfunction. J Neurochem 121(5):830-839.

Wirdefeldt K, Adami HO, Cole P, Trichopoulos D, Mandel J. 2011. Epidemiology and etiology of Parkinson's disease: a review of the evidence. Eur J Epidemiol 26 Suppl 1:S1-58.

VITA

Noah Sorscher was born in Salt Lake City, Utah. He has lived most of his life in Seattle, WA. At Stanford University he earned a Bachelor of Sciences degree in Biology. In 2012 he earned a Doctor of Philosophy at the University of Washington in Neurobiology & Behavior.